

CAMBRIDGE  
UNIVERSITY PRESS

10 July 2011

# Journal of Fluid Mechanics

VOLUME 678



# Multi-component particle-size segregation in shallow granular avalanches

J. M. N. T. GRAY<sup>1</sup>† AND C. ANCEY<sup>2</sup>

<sup>1</sup>School of Mathematics, University of Manchester, Manchester M13 9PL, UK

<sup>2</sup>École Polytechnique Fédérale de Lausanne, Ecublens, 1015 Lausanne, Switzerland

(Received 15 October 2010; revised 30 January 2011; accepted 14 March 2011;  
first published online 31 May 2011)

A general continuum theory for particle-size segregation and diffusive remixing in polydisperse granular avalanches is formulated using mixture theory. Comparisons are drawn to existing segregation theories for bi-disperse mixtures and the case of a ternary mixture of large, medium and small particles is investigated. In this case, the general theory reduces to a system of two coupled parabolic segregation–remixing equations, which have a single diffusion coefficient and three parameters which control the segregation rates between each pair of constituents. Considerable insight into many problems where the effect of diffusive remixing is small is provided by the non-diffusive case. Here the equations reduce to a system of two first-order conservation laws, whose wave speeds are real for a very wide class of segregation parameters. In this regime, the system is guaranteed to be non-strictly hyperbolic for all admissible concentrations. If the segregation rates do not increase monotonically with the grain-size ratio, it is possible to enter another region of parameter space, where the equations may either be hyperbolic or elliptic, depending on the segregation rates and the local particle concentrations. Even if the solution is initially hyperbolic everywhere, regions of ellipticity may develop during the evolution of the problem. Such regions in a time-dependent problem necessarily lead to short wavelength Hadamard instability and ill-posedness. A linear stability analysis is used to show that the diffusive remixing terms are sufficient to regularize the theory and prevent unbounded growth rates at high wave numbers. Numerical solutions for the time-dependent segregation of an initially almost homogeneously mixed state are performed using a standard Galerkin finite element method. The diffuse solutions may be linearly stable or unstable, depending on the initial concentrations. In the linearly unstable region, ‘sawtooth’ concentration stripes form that trap and focus the medium-sized grains. The large and small particles still percolate through the avalanche and separate out at the surface and base of the flow due to the no-flux boundary conditions. As these regions grow, the unstable striped region is annihilated. The theory is used to investigate inverse distribution grading and reverse coarse-tail grading in multi-component mixtures. These terms are commonly used by geologists to describe particle-size distributions in which either the whole grain-size population coarsens upwards, or just the coarsest clasts are inversely graded and a fine-grained matrix is found everywhere. An exact solution is constructed for the steady segregation of a ternary mixture as it flows down an inclined slope from an initially homogeneously mixed inflow. It shows that for distribution grading, the particles segregate out into three inversely graded sharply segregated layers sufficiently far downstream, with the largest particles on top, the fines at the bottom and the medium-sized grains sandwiched in between. The heights of the

† Email address for correspondence: nico.gray@manchester.ac.uk

layers are strongly influenced by the downstream velocity profile, with layers becoming thinner in the faster moving near-surface regions of the avalanche, and thicker in the slowly moving basal layers, for the same mass flux. Conditions for the existence of the solution are discussed and a simple and useful upper bound is derived for the distance at which all the particles completely segregate. When the effects of diffusive remixing are included, the sharp concentration discontinuities are smoothed out, but the simple shock solutions capture many features of the evolving size distribution for typical diffusive remixing rates. The theory is also used to construct a simple model for reverse coarse-tail grading, in which the fine-grained material does not segregate. The numerical method is used to calculate diffuse solutions for a ternary mixture and a sharply segregated shock solution is derived that looks similar to the segregation of a bi-disperse mixture of large and medium grains. The presence of the fine-grained material, however, prevents high concentrations of large or medium particles being achieved and there is a significant lengthening of the segregation distance.

**Key words:** granular media, multiphase flow, shock waves

---

## 1. Introduction

Polydisperse granular materials are extremely common in our kitchens, in our natural environment, as well as in many industrial, pharmaceutical, chemical and agricultural processes. Particles rarely have a regular shape or a uniform size distribution, and it is technologically challenging to produce a very high tolerance monodisperse mixture of spherical grains, which is the implicit assumption in many granular theories. As multi-component mixtures are moved, stored, agitated or allowed to flow, they have a tendency to segregate. This can sometimes be desirable, such as in mining and stone crushing, and can be exploited to separate the grains into approximately monodisperse size classes (Wills 1979), but it is often a source of great frustration that can significantly degrade the quality and the safety of a product (Johanson 1978). A considerable amount of early work was therefore performed by engineers who sought to understand the fundamental size segregation mechanisms and learn how to control their effects (Williams 1968; Bridgwater 1976; Drahn & Bridgwater 1983). Geologists and sedimentologists were also early pioneers who were quick to identify inversely (or reverse) graded deposits, in which the grain-size population coarsens upwards, and use this as an indicator of ancient granular avalanches on dunes, in dense pyroclastic flows and debris flows (e.g. Bagnold 1954; Middleton 1970; Middleton & Hampton 1976). As many as 13 different segregation mechanisms for dissimilar grains have now been identified (McCarthy 2009), with the primary ones being percolation (e.g. Middleton 1970; Scott & Bridgwater 1975), trajectory segregation (e.g. Schulze 2008), convection (e.g. Ehrichs *et al.* 1995) and fluidization (e.g. Schröter *et al.* 2006).

In shallow granular avalanches it is widely accepted that void-filling percolation is the dominant mechanism for size segregation (Savage & Lun 1988; Vallance & Savage 2000). This is the process in which random fluctuations within the flowing avalanche constantly open up gaps and the smaller particles are statistically more likely to drop down into them, under the action of gravity, than the large ones, because they are more likely to fit into the available space. This void-filling process has also been termed kinetic sieving (Middleton 1970) and Savage & Lun (1988)

identified the related process of squeeze expulsion, which describes the forces that the small particles exert on the large grains, once they are underneath, that lever them up towards the surface of the flow. This percolation mechanism is extremely efficient in dry granular flows, with the large ones rising to the surface even when there are only small size differences between the particles, and even when the large particles are significantly denser than the small ones (Rosato *et al.* 1987).

Granular avalanches, and the segregation that they induce, are much more widespread than one might think. They occur on geophysical scales in the form of snow avalanches (Savage & Hutter 1989; Jomelli & Bertran 2001; Bartelt & McArdell 2009), rockfalls (Dade & Huppert 1998; Bertran 2003), dense pyroclastic flows (Branney & Kokelaar 1992; Calder, Sparks & Gardeweg 2000) and debris flows (Costa & Williams 1984; Pierson 1986; Iverson 1997; Iverson & Vallance 2001), as well as on much smaller scales in the form of chute flows (Gray, Wieland & Hutter 1999; Khakhar, McCarthy & Ottino 1999), during the formation of heaps (Williams 1968; Gray & Hutter 1997; Makse *et al.* 1997), in the filling of hoppers (Baxter *et al.* 1998) and in rotating drums (Gray & Hutter 1997; Khakhar, McCarthy & Ottino 1997; Hill *et al.* 1999; Hill, Gioia & Amaravadi 2004; Zuriguel *et al.* 2006). As the particle-size distribution evolves within these flows, there can be interesting feedbacks on the bulk flow itself (Phillips *et al.* 2006; Rognon *et al.* 2007; Gray & Ancy 2009). For instance, Pouliquen, Delour & Savage (1997) and Pouliquen & Vallance (1999) showed that if the large particles are rougher, or more resistive, than the small grains, the flow can develop frontal instabilities, which leads to the formation of fingers and coarse-grained lateral levees that channelize the flow and significantly enhance runout distances (Gray & Kokelaar 2010*a, b*). This is particularly important for hazardous geophysical flows, such as snow avalanches and debris flows (Jomelli & Bertran 2001; Iverson & Vallance 2001), where extended runouts can impact on populated areas.

Avalanches often occur as part of complex granular flows that also have regions of slowly moving or static grains, such as in the rotating drum experiment shown in figure 1. Here the vast majority of the grains are in slow solid-body rotation, but there is a thin steadily flowing avalanche along the inclined free surface. The avalanche has a maximum depth of 7 mm and continuously erodes material on the upper half of the slope and deposits it along the lower half (e.g. Gray 2001). All the segregation occurs within the avalanche. As the drum is rotated clockwise, the initially homogeneous mixture of three particle-size classes is rotated towards the free surface and is entrained into the avalanche. Within it, the large- and medium-sized grains rise upwards due to size segregation until they reach a level where they are surrounded by high concentrations of their own particle type and the segregation stops. Small particles that are entrained along the upper reaches of the avalanche are already in a high concentration basal region of small particles and do not rise upwards, nor do they percolate back into the slowly rotating material beneath because there is insufficient dilatation. Very rapidly, three inversely graded layers form, with high concentrations of large green particles (500–750  $\mu\text{m}$ ) at the top, high concentrations of small pink particles (75–150  $\mu\text{m}$ ) at the bottom and a layer of white medium-sized grains (400–500  $\mu\text{m}$ ) sandwiched in between, as shown in the close-up photograph in figure 2. This is an example of what geologists call inverse distribution grading, where all the particle sizes segregate in the flow and coarsen upwards (Middleton & Hampton 1976; Cas & Wright 1987; Hiscott 2003).

In the lower reaches of the drum, where the material is rotating away from the steady avalanche, the small grains are stripped off the bottom of the flow first and are

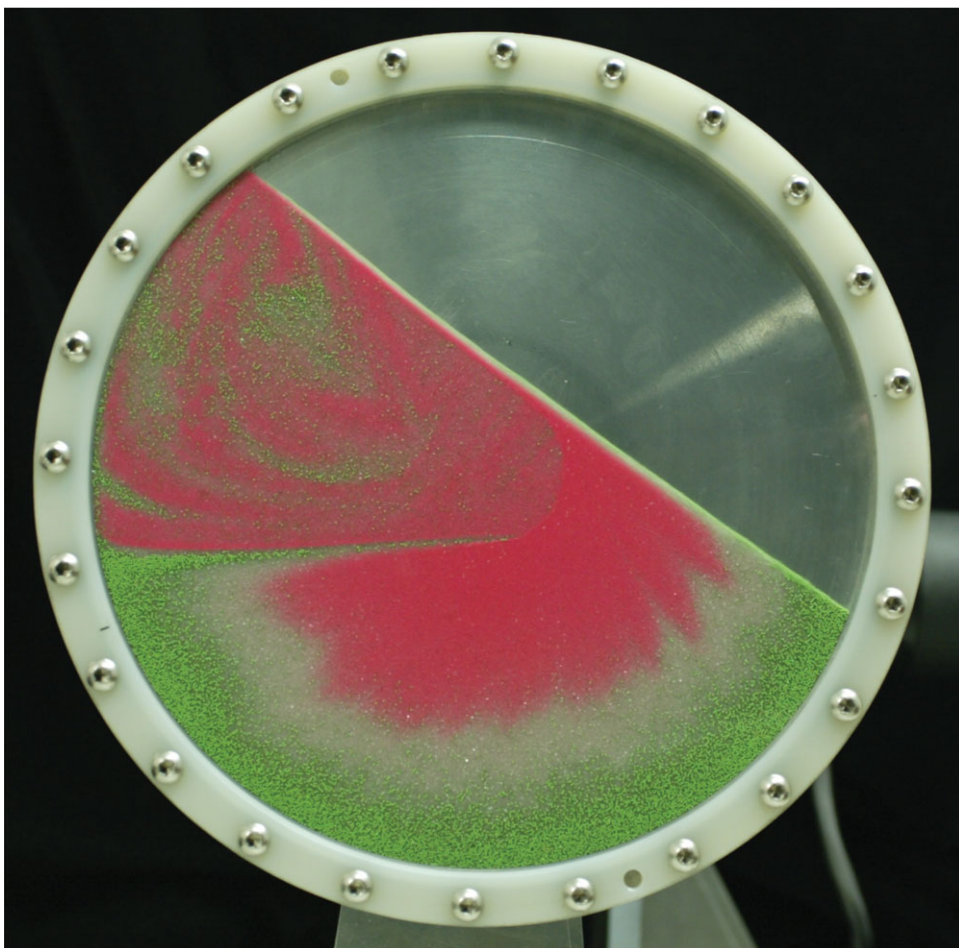


FIGURE 1. Segregation of a three-phase mixture in a 24.5 cm diameter drum with a 3 mm gap rotating at 0.68 revolutions per minute. The green particles are 500–750  $\mu\text{m}$ , the white particles are 400–500  $\mu\text{m}$  and the pink particles are 75–150  $\mu\text{m}$  in size. Initially, they are approximately homogeneously mixed, which can be seen in the undisturbed solid rotating material on the upper left-hand side of the drum. As the drum rotates clockwise, this region is entrained into a thin continuously flowing avalanche close to the free surface and is rapidly segregated as it flows downslope. Even over this short distance, inversely graded layers form in the avalanche, with the largest green particles on top, the smallest pink ones at the bottom and the white middle-sized grains sandwiched in between, as shown in figure 2. As the particles are continuously deposited into the solid rotating body of grains underneath, the largest particles, at the top of the avalanche, are the last to get deposited and therefore end up adjacent to the drum wall. While the smallest grains at the base of the avalanche are the first to get deposited closest to the centre of the drum, the medium grains are deposited in a band in between the two. This gives rise to a radial segregation pattern in the region of particles that have already passed through the avalanche, which contrasts strongly with the homogeneous region that is yet to be entrained.

progressively deposited until there are none left. The medium-sized grains are next to deposit in a medial band and finally the large pink grains deposit last close to the drum wall. This creates what is called a radial segregation pattern in the slowly rotating deposit. Figure 1 shows the segregation after the drum has rotated through an angle of 130°. In the top left of the deposit, the initially homogeneous mixture



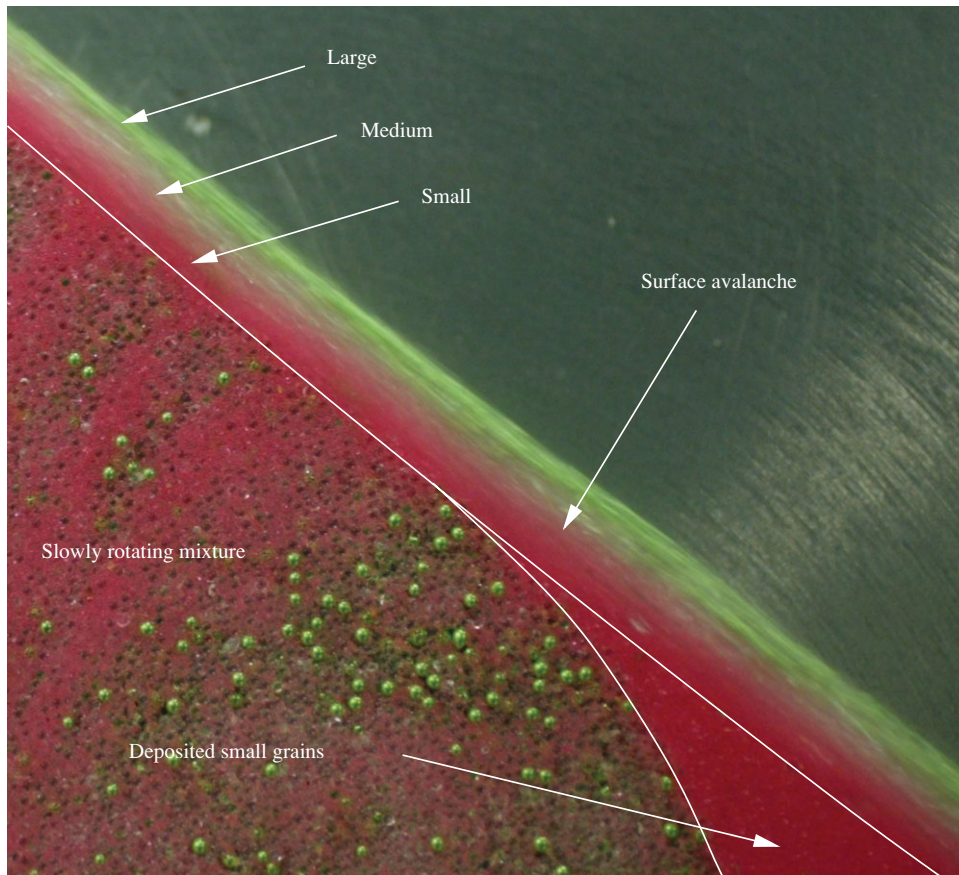


FIGURE 2. Close-up photograph of the segregation within the surface avalanche in the thin rotating drum experiment shown in figure 1. The segregation is strong enough that the avalanche rapidly develops an inversely graded particle-size distribution, with the large green particles ( $500\text{--}750\text{ }\mu\text{m}$ ) on top, the small pink particles ( $75\text{--}150\text{ }\mu\text{m}$ ) at the bottom and the medium-sized white grains ( $400\text{--}500\text{ }\mu\text{m}$ ) sandwiched in between. In the upper reaches of the avalanche the initial mixture of grains is rotated towards the free surface and entrained, while in the lower reaches the grains are deposited. Since the small particles are concentrated at the bottom of the avalanche they are deposited first.

of grains that is being rotated towards the free surface is still visible, and in the remaining region the partially formed radial segregation pattern can be seen. The contrast between the radial size distribution and the initial distribution is striking and indicates how strong the percolation process can be even over relatively short distances.

Geologists and sedimentologists encounter very complicated mixtures of particles of varying sizes and densities that are deposited from both granular and granular fluid flows. They have become expert at interpreting such deposits, as well as the flows and the depositional processes that gave rise to them. In terms of geological nomenclature, the radial pattern formed in the deposit is a result of progressive aggradation of the grains from the flowing avalanche (Branney & Kokelaar 1992). Rather interestingly, the large-scale deposited pattern is not inversely graded, even though it is formed from a flow that is strongly inversely graded. At lower rotation rates it is possible to deposit the grains en masse by the upward propagation of a granular shock wave

(Gray & Kokelaar 2010*a, b*), which leaves stripes of inversely graded material in the deposit. At high and low drum fill levels, this can lead to Catherine wheel (Gray & Hutter 1997) and palm leaf (Gray & Chugunov 2006) patterns. At 50 % fill, petals can form (Hill *et al.* 2004; Zuriguel *et al.* 2006) by segregation-mobility feedback effects within the avalanche. The final deposits are therefore far from representative of the segregation within the flowing avalanche and strongly reflect the mode and timing of the deposition.

Newey *et al.* (2004) have performed experiments in a long rotating drum and shown that radial segregation developed with all the mixtures that they tried, which had between three and six particle sizes. With a three-constituent mixture, axial bands also developed after about 5 min, and the smallest particles formed bands inside the bands of medium and large grains. The ternary mixture also had a much richer dynamics than the equivalent bi-disperse case (Hill & Kakalios 1995). Curiously, they found that axial bands did not form when five or more particle sizes were present, which suggests that strongly polydisperse mixtures mitigate some of the effects of segregation. This is potentially significant, especially if continuously distributed granular materials can be engineered to significantly reduce or eliminate segregation in practical industrial processes without having to include cohesive or other effects (e.g. Jha & Puri 2010; McCarthy 2009).

As well as distribution grading, there is also another form of inverse grading that geologists call reverse coarse-tail grading (see e.g. Cas & Wright 1987; Branney & Kokelaar 1992; Palladino & Valentine 1995; Hiscott 2003). This describes the situation in which a certain proportion of the coarse clasts, the coarse tail, are inversely graded and the remaining fine-grained material is poorly sorted and found throughout the deposit. This is a common feature of pyroclastic flow deposits (e.g. Branney & Kokelaar 1992; Calder *et al.* 2000), where the large low-density pumice clasts are commonly found on the free surface of the deposit. There is still considerable debate in the literature about the dominant mechanism for segregation in this case. One hypothesis is that the motion of the finer-grained material is driven by fluidizing air or water, which occupies the interstices, whereas the larger grains segregate by percolation. Alternatively, laboratory experiments (Shinbrot & Muzzio 1998; Cagnoli & Manga 2005) suggest that in a strongly agitated flow, the larger grains might also be driven by buoyancy effects in a matrix of finer-grained material. This may lead to either reverse or normal coarse-tail grading, depending on the density of the large grains. However, it is important to add the caveat that deposits observed in the field may be more a function of complex waxing and waning phases of the avalanche and the associated depositional regimes (Branney & Kokelaar 1992) than being representative of the size distribution within the parent flow.

Although there have been several recent studies of multi-component segregation in both wet and dry granular materials, in the geological (Cagnoli & Manga 2005), hydraulics (Zanuttigh & Di Paolo 2006; Zanuttigh & Ghilardi 2010) and engineering (Jha & Puri 2010) communities, the field currently lacks a basic theoretical framework to guide it further. This paper seeks to address this issue, by deriving a multi-component size segregation theory for polydisperse granular mixtures. Despite the apparent complexity of the problem, the theory is capable of describing the evolution of the size distribution towards an ‘inversely graded’ steady state, in which the whole grain-size population coarsens upwards, as well as the development of ‘reverse coarse-tail grading’ where just the coarse tail of the population is inversely graded and the fine-grained matrix is found everywhere. The resulting systems of parabolic segregation–remixing equations can easily be solved by existing programme libraries,

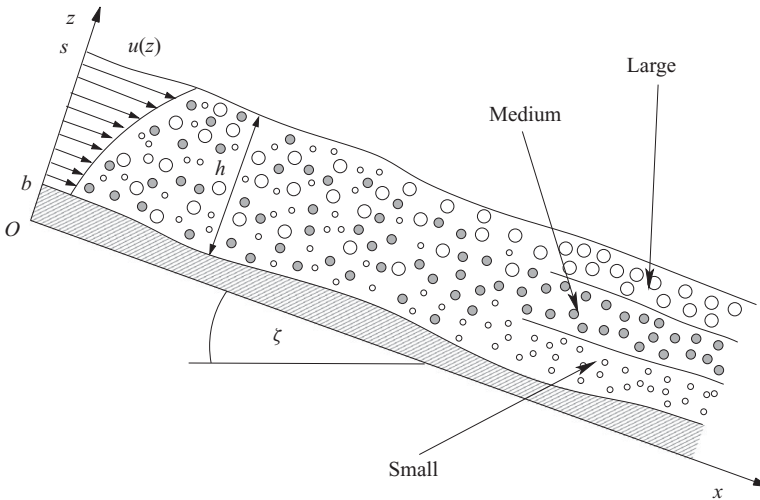


FIGURE 3. A schematic diagram of the particle-size segregation in an avalanche with three particle sizes. At the origin  $O$  the particles enter in a homogeneously mixed state, but as they avalanche down slope, the large grains gradually rise to the surface, the small ones percolate down to the base and the medium-sized grains are sandwiched in between. This creates three inversely graded layers sufficiently far downstream. The downstream coordinate  $x$  is inclined at an angle  $\zeta$  to the horizontal, the  $y$  coordinate is into the page and  $z$  is the upward-pointing normal. The avalanche free surface lies at  $z = s$ , the base is at  $z = b$  and the avalanche thickness  $h = s - b$ . The arrows on the left-hand side indicate the downstream velocity profile  $u(z)$  through the avalanche.

which makes the theory readily accessible to the wide range of disparate communities where size segregation is important.

This paper is structured as follows. The multi-component theory is formulated in §2 and compared with existing bi-disperse theories in §3. In §§4 and 5 the ternary mixture equations are investigated. It is shown that in the absence of diffusion, the system can be ill-posed if the segregation rate does not rise monotonically with the grain-size ratio. The addition of diffusive remixing is sufficient to regularize the model, but instabilities may still develop (§6) and can lead to ‘sawtooth’ segregation stripes (§7). In §§8–10 exact and numerical solutions are constructed for both inverse distribution grading and reverse coarse-tail grading, which will be of considerable interest to geologists and sedimentologists. A short matlab code to solve the ternary segregation–remixing equations using pdepe is included in the online supplementary material available at [journals.cambridge.org/flm](http://journals.cambridge.org/flm).

## 2. Derivation from multi-component mixture theory

### 2.1. Mixture framework

Consider a multi-component mixture of particles of differing sizes that flows down a chute inclined at an angle  $\zeta$  to the horizontal, as shown in figure 3. A coordinate system  $Oxyz$  is defined with the  $x$ -axis pointing down the chute, the  $y$ -axis pointing across the chute and the  $z$ -axis being the upward-pointing normal. All the particles, regardless of the size class that they lie in, are assumed to have the same intrinsic



density

$$\rho^{\nu*} = \rho, \quad \forall \nu, \quad (2.1)$$

where the superscript  $\nu$  denotes a class of particles of a given size and the superscript  $*$  is used to indicate an intrinsic variable, which is defined per unit volume of a pure phase of that constituent.

Following Gray & Thornton (2005) the interstitial pore space is incorporated into each phase, which implicitly assumes that the solids volume fraction is uniform and constant, and that the density of any pore fluid is negligible (Thornton, Gray & Hogg 2006). In real granular materials, the solids volume fraction can be non-uniform and may evolve in time. In particular, when there is a mixture of grains of varying sizes, the smaller ones can fill the gaps between the larger ones and enhance the packing density. Golick & Daniels (2009) were able to use this effect to infer the progress of segregation in their bi-disperse annular shear cell experiments. They found that the position of their top plate changed by about 2.5 % of the flow height, as the large and small grains readjusted from an initially segregated unstably stratified configuration, to a denser mixed state and then to a stably segregated state again. It is known that static Apollonian packings can approach 100 % solids volume fraction (Herrmann, Mantica & Bessis 1990), but almost nothing is known about changes in packing density in polydisperse sheared systems. Assuming that the solids volume fraction is constant and uniform is therefore a reasonable first approximation, which might be improved upon in future.

Mixture theory defines overlapping partial densities,  $\rho^\nu$ , partial velocities,  $\mathbf{u}^\nu$ , and partial pressures,  $p^\nu$ , for each constituent  $\nu$  (Truesdell 1984; Morland 1992). Equally important are the volume fractions, which describe how the space is shared between the constituents. The concentration  $\phi^\nu$  is defined as the volume fraction of constituent  $\nu$  per unit volume of mixture and lies in the range

$$0 \leq \phi^\nu \leq 1. \quad (2.2)$$

The sum over all constituents is necessarily equal to unity

$$\sum_{\forall \nu} \phi^\nu = 1. \quad (2.3)$$

In standard mixture theory, the partial and intrinsic velocity fields are identical, but the other fields such as the density, Cauchy stresses and pressures are usually related by a linear volume fraction scaling

$$\rho^\nu = \phi^\nu \rho^{\nu*}, \quad \mathbf{T}^\nu = \phi^\nu \mathbf{T}^{\nu*}, \quad p^\nu = \phi^\nu p^{\nu*}, \quad \mathbf{u}^\nu = \mathbf{u}^{\nu*}. \quad (2.4)$$

The bulk density  $\rho$  and the bulk pressure  $p$  are defined as the sum of the partial densities and partial pressures:

$$\rho = \sum_{\forall \nu} \rho^\nu, \quad p = \sum_{\forall \nu} p^\nu. \quad (2.5)$$

Each constituent satisfies individual mass

$$\frac{\partial \rho^\nu}{\partial t} + \nabla \cdot (\rho^\nu \mathbf{u}^\nu) = 0 \quad (2.6)$$

and momentum

$$\frac{\partial}{\partial t}(\rho^\nu \mathbf{u}^\nu) + \nabla \cdot (\rho^\nu \mathbf{u}^\nu \otimes \mathbf{u}^\nu) = \nabla \cdot \mathbf{T}^\nu + \rho^\nu \mathbf{g} + \boldsymbol{\beta}^\nu \quad (2.7)$$

balance laws, where  $\otimes$  is the dyadic product and  $\mathbf{g}$  is the gravitational acceleration vector. The interaction force,  $\boldsymbol{\beta}^\nu$ , is the force exerted on phase  $\nu$  by all the other constituents. These interaction forces sum to zero over all constituents

$$\sum_{\forall \nu} \boldsymbol{\beta}^\nu = \mathbf{0}. \quad (2.8)$$

Following Gray, Tai & Noelle (2003), the stress tensor  $\mathbf{T}^\nu = -p^\nu \mathbf{1} + \boldsymbol{\sigma}^\nu$  is broken down into a spherical pressure  $-p^\nu \mathbf{1}$  and a deviatoric stress  $\boldsymbol{\sigma}^\nu$ , where  $\mathbf{1}$  is the unit tensor. It is assumed that in the normal direction the pressure dominates, and the deviatoric stresses and the normal acceleration terms can be neglected. This implies that the normal components of the momentum balances (2.7) sum to

$$\frac{\partial p}{\partial z} = -\rho g \cos \zeta, \quad (2.9)$$

over all constituents, where  $g$  is the constant of gravitational acceleration. As the bulk density is constant and the avalanche free surface,  $z = s$ , is traction-free, (2.9) can be integrated through the avalanche depth, subject to the condition that  $p(s) = 0$ , to show that the pressure is lithostatic,

$$p = \rho g(s - z) \cos \zeta. \quad (2.10)$$

This ensures compatibility with most existing avalanche models (e.g Grigorian, Eglit & Iakimov 1967; Savage & Hutter 1989; Iverson 1997; Gray *et al.* 1999; Pouliquen 1999a; Iverson & Denlinger 2001; Gray *et al.* 2003; Pitman *et al.* 2003; Gruber & Bartelt 2007; Mangeney *et al.* 2007).

## 2.2. Derivation of the percolation velocity

It is surprisingly easy to generalize Gray & Thornton's (2005) derivation to multiple constituents of different sized particles. In their two-constituent formulation, they assumed that as small particles percolated downwards under gravity, they supported less of the overburden pressure and consequently the large grains needed to support more of the load. This led them to introduce a relation between the partial and intrinsic pressures that differed from standard mixture theory (2.4). Their partial pressure relation generalizes naturally to multiple constituents and is given by

$$p^\nu = f^\nu p, \quad (2.11)$$

where the factor  $f^\nu$  determines the proportion of the lithostatic pressure carried by each constituent  $\nu$ . Summing the partial pressure (2.11) over all constituents and using (2.5) implies that the  $f^\nu$  factors must sum to unity,

$$\sum_{\forall \nu} f^\nu = 1. \quad (2.12)$$

We shall adopt the same form for the interaction drag law  $\boldsymbol{\beta}^\nu$  that was proposed by Gray & Chugunov (2006), which consists of three terms

$$\boldsymbol{\beta}^\nu = p \nabla f^\nu - \rho^\nu c(\mathbf{u}^\nu - \mathbf{u}) - \rho d \nabla \phi^\nu, \quad (2.13)$$

where  $c$  is the coefficient of interparticle drag,  $d$  is the coefficient of diffusive remixing and  $\mathbf{u}$  is the barycentric or bulk velocity defined by

$$\rho \mathbf{u} = \sum_{\forall \nu} \rho^\nu \mathbf{u}^\nu. \quad (2.14)$$

The first term in (2.13) combines with the pressure gradient in (2.7) to ensure that the percolation process is driven by the intrinsic rather than the partial pressure gradient, the second provides a linear resistance to relative motions and the third is a concentration gradient-dependent force that was used to model diffusive remixing of the particles. The interaction drag  $\beta^v$  has been constructed so that it automatically satisfies the summation condition (2.8) and it assumes that the drag and diffusive remixing coefficients are the same for all phases.

The bulk velocity  $\mathbf{u}$  has components  $u$ ,  $v$  and  $w$  in the downslope, cross-slope and normal directions, respectively. The percolation velocities due to segregation, relative to the bulk flow, in the down slope and cross-slope directions are typically much smaller than the magnitude of the bulk velocity itself. The constituent velocities,  $u^v$  and  $v^v$ , in these directions are therefore assumed to be equal to the bulk velocity components,

$$u^v = u, \quad v^v = v. \quad (2.15)$$

The velocity components in the normal direction can be calculated by substituting (2.4), (2.9), (2.11) and (2.13) into the normal component of the momentum balance (2.7). Assuming that the normal accelerations are negligible implies that

$$\phi^v w^v = \phi^v w + (f^v - \phi^v)(g/c) \cos \zeta - (d/c) \frac{\partial \phi^v}{\partial z}, \quad (2.16)$$

which is precisely the same as the equation obtained by Gray & Chugunov (2006). For the segregation process, the crucial part of this equation is the difference in the factors  $f^v$  and  $\phi^v$ . In the absence of diffusion ( $d=0$ ), if  $f^v > \phi^v$  then the particles will rise, if  $f^v < \phi^v$  the particles will fall and if  $f^v = \phi^v$  there will be no motion relative to the bulk. Gray & Thornton (2005) motivated the form of  $f^v$  on the basis that when small particles were percolating downwards, the large grains must support more of the overburden pressure and consequently  $f^v > \phi^v$ . There are two constraints on this. Firstly, when any class of particles are in a pure phase they must carry all of the load

$$f^v = 1, \quad \text{when } \phi^v = 1, \quad \text{or equivalently,} \quad \text{when } \phi^\mu = 0, \quad \forall \mu \neq v, \quad (2.17)$$

and secondly, when there are no particles of that phase, they cannot carry any of the load

$$f^v = 0, \quad \text{when } \phi^v = 0. \quad (2.18)$$

A significant generalization of the factors  $f^v$  is required for the multi-component theory. Motivated by the fact that if any two constituents are found in isolation, the form of  $f^v$  must reduce to that proposed by Gray & Thornton (2005), an additive decomposition of the form

$$f^v = \phi^v + \sum_{\forall \mu} B_{v\mu} \phi^v \phi^\mu \quad (2.19)$$

is assumed, where the non-dimensional parameter  $B_{v\mu}$  determines the magnitude of the pressure perturbation for constituent  $v$  due to the presence of constituent  $\mu$ . Although more general functional forms are possible, this is the simplest that automatically satisfies the constraints (2.17) and (2.18). If, in addition, there are no pressure perturbations exerted by any constituent on itself

$$B_{(vv)} = 0, \quad \forall v, \quad (2.20)$$

and the pressure perturbation on constituent  $\nu$  due to constituent  $\mu$  is equal and opposite to the pressure perturbation on constituent  $\mu$  by constituent  $\nu$ ,

$$B_{\nu\mu} = -B_{\mu\nu}, \quad \forall \nu \neq \mu, \quad (2.21)$$

then the summation condition (2.12) is automatically satisfied as well. The matrix  $\mathbf{B}$  formed by the coefficients  $B_{\nu\mu}$  has the interesting property that it is antisymmetric, i.e.  $\mathbf{B} = -\mathbf{B}^T$ , where the superscript T denotes the transpose.

An equation for the normal velocity of constituent  $\nu$  can be obtained by substituting (2.19) into (2.16) and dividing through by  $\phi^\nu$  to give

$$w^\nu = w + \sum_{\forall \mu} q_{\nu\mu} \phi^\mu - D \frac{\partial}{\partial z} (\ln \phi^\nu), \quad (2.22)$$

where  $q_{\nu\mu}$  is the maximum segregation velocity of phase  $\nu$  relative to phase  $\mu$ , and  $D$  is the diffusivity. These are defined as

$$q_{\nu\mu} = B_{\nu\mu}(g/c) \cos \zeta, \quad D = d/c, \quad (2.23)$$

respectively. In the absence of diffusion, the segregation stops whenever the particles are in a pure phase, since  $\phi^\nu = 1$  necessarily implies that  $\phi^\mu = 0$  for  $\mu \neq \nu$  in (2.22). The normal velocity,  $w^\nu$ , is then equal to the bulk velocity,  $w$ .

While mixture theory sets up a framework within which to model particle-size segregation, it does not yield any further information about the functional dependence of the maximum segregation velocities  $q_{\nu\mu}$ , or the diffusivity  $D$ , on the particle-size ratio, the shear rate, the dilatation or any other variables. These must be determined by experiment or from particle dynamics simulations. There has, however, been some recent progress in determining these parameters for bi-disperse mixtures. Golick & Daniels (2009) and May *et al.* (2010) have measured the time scale for segregation  $t_s$  in an annular shear cell, with different particle-size ratio mixtures. Instead of a linear dependence, as one might anticipate, they found that there was a minimum  $t_s$  when the large grains were twice the size of the small particles. This is a very interesting and important finding, which suggests that the maximum segregation velocity  $q_{ls}$  for a bi-disperse mixture should have a local maximum at a grain-size ratio of two as illustrated schematically in figure 4(a). At present, it is unclear whether the segregation velocity will begin to increase again at some point after the local maximum (as illustrated) or whether it continues to decrease with increasing particle-size ratio.

One of the key advantages of the linear decomposition (2.19) is that the bi-disperse maximum segregation velocity curve, which is sketched in figure 4(a–d) for different grain-size ratios, can be used to determine the segregation rates in multi-component mixtures. This is a potentially very significant and practical simplification. For example, for a three-component mixture composed of large, medium and small particles denoted by the constituent letters  $\nu = l, m, s$ , respectively, a monotonically increasing curve would imply that the segregation velocity of the large and small particles,  $q_{ls}$ , was always larger than the segregation velocities,  $q_{lm}$  and  $q_{ms}$ , of the large and medium grains, and the medium and small grains, as shown in figure 4(c). However, if  $q_{\nu\mu}$  has a local maximum at a grain-size ratio of two, the particle-size ratios can be picked so that  $q_{ms} \geq q_{ls} \geq q_{lm}$  as in figure 4(a), or so that  $q_{lm} \geq q_{ls} \geq q_{ms}$  as in figure 4(b), or even so that both  $q_{lm}$  and  $q_{ms}$  are larger than  $q_{ls}$  as in figure 4(d). It shall be shown in this paper that this final condition can lead to the linear instability of an initially homogeneously mixed three-component mixture.

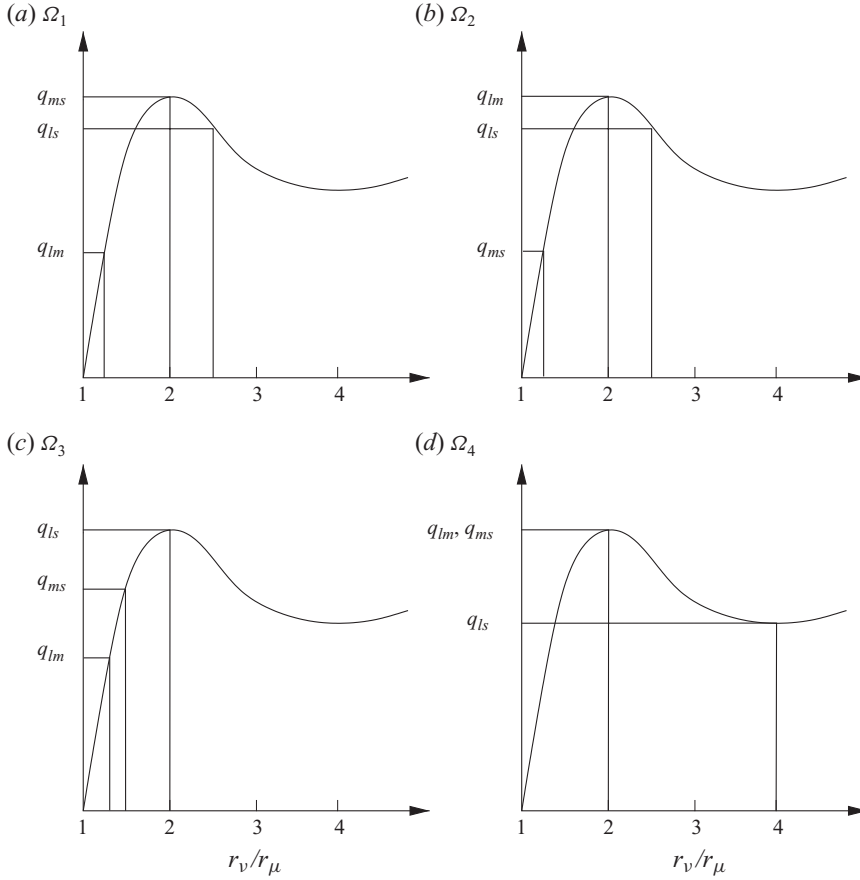


FIGURE 4. A sketch of the maximum segregation velocity  $q_{v\mu}$  as a function of the grain-size ratio  $r_v/r_\mu$ , where the grain size  $r_v$  is assumed to be larger than  $r_\mu$ . The curve is assumed to have a maximum at a grain-size ratio of two. The resulting maximum segregation velocities are illustrated for a three-component mixture of large, medium and small particles denoted by the constituent letters  $v = l, m, s$ , and various grain-size ratio combinations. There are four basic states (a–d) if there is a local maximum in  $q_{v\mu}$ . In (a)  $r_m/r_s = 2$  and  $r_l/r_s = 5/2$ , which necessarily implies  $r_l/r_m = 5/4$  and  $q_{ms} \geq q_{ls} \geq q_{lm}$ . In (b)  $r_l/r_m = 2$  and  $r_l/r_s = 5/2$ , so  $r_m/r_s = 5/4$  and  $q_{lm} \geq q_{ls} \geq q_{ms}$ . In (c),  $r_l/r_s = 2$  and  $r_m/r_s = 3/2$ , and hence  $r_l/r_m = 4/3$ , which implies that  $q_{ls}$  is larger than the other segregation rates. However, in (d)  $r_m/r_s = 2$  and  $r_l/r_m = 2$ , so  $r_l/r_s = 4$ , and  $q_{ls}$  is less than the other segregation rates. The regimes are denoted  $\Omega_1$ – $\Omega_4$ .

At present, a curve similar to that shown in figure 4(a) has not been measured, but there is progress towards this goal. Wiedersseiner *et al.* (2011) have performed a series of steady two-dimensional chute flow experiments in a narrow channel inclined at  $29^\circ$  with mixtures of 2 mm and 1 mm particles. The experiments used an unstably stratified inflow condition (Gray & Chugunov 2006) that allowed the relative discharge rates to be varied. The experiments were photographed 2000 times at the sidewall to create a time-averaged picture, which could then be mapped to the particle concentration. By performing this at a series of stations, they were able to build up a composite picture of the evolving concentration distribution along the chute. Wiedersseiner *et al.* (2011) were able to determine values for the maximum segregation rate and the diffusivity, by comparison with numerical solutions of the theory of Gray & Chugunov (2006).



In order to get good agreement with the inversely graded steady uniform state far downstream, they found that the maximum segregation velocity  $q_{ls}$  and diffusivity  $D$  could be taken to be independent of depth, but it was very important to use the exponential downstream velocity profile  $u(z)$  that they measured in their experiments. For a range of inflow conditions, Wiederseiner *et al.* (2011) found that the maximum segregation velocity,  $q_{ls}$ , was in the range of 1.23–1.99 mm s<sup>−1</sup> and the diffusivity,  $D$ , was between 2.08 and 2.79 mm<sup>2</sup> s<sup>−1</sup>. This contrasts with previous studies (e.g. Scott & Bridgwater 1975; Golick & Daniels 2009; May *et al.* 2010), which show that the maximum segregation rate  $q_{ls}$  can be dependent on shear rate and have pressure dependence. This apparent disagreement may simply be an indication that once sufficient dilatation has occurred for the grains to percolate freely, the shear rate and pressure dependence diminishes.

### 2.3. Non-dimensionalization and the segregation–remixing equation

Following Gray & Thornton (2005) it is convenient to introduce non-dimensional variables using scalings that reflect the shallowness of the avalanche

$$x = L\hat{x}, \quad z = H\hat{z}, \quad (u, v) = U(\hat{u}, \hat{v}), \quad (w, w^v) = \frac{HU}{L}(\hat{w}, \hat{w}^v), \quad t = \frac{L}{U}\hat{t}, \quad (2.24)$$

where  $L$  is a typical downstream length scale,  $H \ll L$  is a typical thickness and  $U$  is a typical downstream velocity magnitude. The horizontal length scale  $L$  and the velocity magnitude  $U$  have been left as general as possible to encompass the scalings used on both smooth and rough beds (Savage & Hutter 1989; Pouliquen 1999*a, b*; Gray & Ancey 2009). Substituting the scalings into (2.22) implies that the non-dimensional normal velocity of constituent  $v$  is

$$w^v = w + \sum_{\forall \mu} S_{v\mu} \phi^\mu - D_r \frac{\partial}{\partial z} (\ln \phi^v), \quad (2.25)$$

where the hats have been dropped for simplicity. The non-dimensional segregation rates  $S_{v\mu}$  and the non-dimensional diffusion coefficient are

$$S_{v\mu} = \frac{L}{HU} q_{v\mu}, \quad D_r = \frac{DL}{H^2 U}. \quad (2.26)$$

The matrix  $\mathbf{S}$  formed by the segregation coefficients  $S_{v\mu}$  is also antisymmetric, since it is proportional to  $\mathbf{B}$  through (2.23) and (2.26). This antisymmetry property means that it is necessary to specify a total number of

$$N_j = \frac{1}{2} j(j-1) \quad (2.27)$$

segregation coefficients for a mixture of  $j$  components. An evolution equation for the concentration of each phase  $v$  is obtained by substituting the normal velocity (2.25) into the non-dimensionalized mass balance equation (2.6) with the downstream and cross-stream velocity given by (2.15). The non-dimensional segregation–remixing equation for phase  $v$  is therefore

$$\frac{\partial \phi^v}{\partial t} + \nabla \cdot (\phi^v \mathbf{u}) + \frac{\partial}{\partial z} \left( \sum_{\forall \mu} S_{v\mu} \phi^v \phi^\mu \right) = \frac{\partial}{\partial z} \left( D_r \frac{\partial \phi^v}{\partial z} \right), \quad (2.28)$$

where the first term on the left-hand side is the rate of change of the concentration  $\phi^v$  with time, the second describes the transport due to the bulk flow field, the third is due to segregation and the term on the right-hand side accounts for diffusive

remixing of the particles. The equation has been carefully constructed to ensure that the summation conditions (2.3) and (2.12) are automatically satisfied. It follows that when it is summed over all constituents, it yields the incompressibility condition

$$\nabla \cdot \mathbf{u} = 0, \quad (2.29)$$

which, together with the lithostatic pressure distribution through the avalanche depth given by (2.10), is the key assumption underlying most granular avalanche and geophysical mass flow models (e.g. Grigorian *et al.* 1967; Savage & Hutter 1989; Iverson 1997; Gray *et al.* 1999; Pouliquen 1999*a,b*; Iverson & Denlinger 2001; Gray *et al.* 2003; Pitman *et al.* 2003; Gruber & Bartelt 2007; Mangeney *et al.* 2007). The multi-component segregation theory, derived in this paper, is therefore compatible with these depth-averaged theories. The bulk velocity field  $\mathbf{u}$ , required by the multi-component theory, can be reconstructed from the depth-averaged velocity field  $\bar{\mathbf{u}}$ , by using the incompressibility condition (2.29) and assumed downstream and cross-stream velocity profiles with depth, as in Gray & Ancey (2009). Segregation-mobility feedback effects on  $\bar{\mathbf{u}}$  can be included by coupling the basal friction to the evolving concentration distribution (Pouliquen & Vallance 1999; Gray & Kokelaar 2010*a,b*). Alternatively, recent advances in our understanding of the constitutive law in dense granular flows (Jop, Forterre & Pouliquen 2006) also opens up the possibility of coupling the rheology to the evolving concentration distribution directly (Rognon *et al.* 2007). These are vital steps towards the full understanding of segregation-mobility feedback effects, which play a crucial role in fingering instabilities on inclined planes (Pouliquen *et al.* 1997), levee formation in geophysical flows (Jomelli & Bertran 2001; Iverson & Vallance 2001; Iverson 2003; Iverson *et al.* 2010) and stratification patterns in heaps (Williams 1968; Gray & Hutter 1997; Makse *et al.* 1997; Gray & Ancey 2009), as well as banding instabilities (Newey *et al.* 2004) and petal formation (Hill *et al.* 2004; Zuriguel *et al.* 2006) in rotating drums.

The inclusion of segregation-mobility feedback is beyond the scope of this paper, which assumes that the bulk velocity field  $\mathbf{u}$  is prescribed. In the latter case, when there is no feedback, (2.28) forms a system of  $j$ -coupled parabolic equations for the evolving concentration of each of the species  $\nu$ . When the diffusion coefficient  $D_r$  is equal to zero, the equations form a first-order system of conservation laws, and discontinuous solutions, or shocks, may develop. It is therefore important to make a clear distinction between the two systems. In this paper, the diffusive case is referred to as the segregation–remixing equations and the non-diffusive case as the segregation equations.

#### 2.4. Boundary and jump conditions

If there is any form of discontinuity, either in the field variables or the material constants, jump conditions must be applied. These can be derived from an integral form of (2.28) using a limiting argument across a surface of discontinuity, propagating with speed  $v_n$  in the direction of the unit normal  $\mathbf{n}$  to the surface (see e.g. Chadwick 1976). The most general form of the jump condition for constituent  $\nu$  is

$$\llbracket \phi^\nu (\mathbf{u} \cdot \mathbf{n} - v_n) \rrbracket + \left\llbracket \sum_{\forall \mu} S_{\nu\mu} \phi^\nu \phi^\mu \mathbf{k} \cdot \mathbf{n} \right\llbracket = \left\llbracket D_r \frac{\partial \phi^\nu}{\partial z} \mathbf{k} \cdot \mathbf{n} \right\llbracket, \quad (2.30)$$

where  $\mathbf{k}$  is the unit vector normal to the chute and the jump bracket  $\llbracket f \rrbracket = f_+ - f_-$  is the difference of  $f$  evaluated on the forward and rearward sides of the shock, which are denoted by the subscripts ‘+’ and ‘−’ respectively. In the absence of diffusion, the

right-hand side vanishes and the jump conditions reduce to a set of shock conditions that can be used to calculate the motion and jumps across evolving concentration discontinuities which may develop in the first-order system of conservation laws. Equation (2.30) is also useful in formulating the boundary conditions for the diffusive problem at physical boundaries. As an example, consider the free surface of the avalanche  $z = s(x, y, t)$ , which satisfies the kinematic boundary condition

$$\frac{\partial s}{\partial t} + u \frac{\partial s}{\partial x} + v \frac{\partial s}{\partial y} - w = 0, \quad \text{on } z = s(x, y, t), \quad (2.31)$$

when there is no erosion or deposition (see e.g. Savage & Hutter 1989; Gray 2001; Gray *et al.* 2003). This equation is usually derived by defining a function  $F = z - s(x, y, t)$  that is identically zero on the surface. The kinematic boundary condition simply advects the surface with the bulk flow field, i.e.  $\partial F / \partial t + \mathbf{u} \cdot \nabla F = 0$ , which on substitution of  $F$  yields (2.31). In order to apply the jump condition (2.30) at the free surface, the unit normal  $\mathbf{n}$  and the normal velocity  $v_n$  must be defined. The unit normal is simply  $\mathbf{n} = \nabla F / |\nabla F|$ . The normal velocity  $v_n$  can also be used to track the free surface, by advecting it in the direction of the normal, i.e.  $\partial F / \partial t + (v_n \mathbf{n}) \cdot \nabla F = 0$ . It is then easy to show that  $v_n = \mathbf{u} \cdot \mathbf{n}$  and hence that the first jump-bracketed term in (2.30) is identically zero. Since there are no small particles outside the avalanche, both  $\phi_+^v$  and  $\partial \phi_+^v / \partial z$  are equal to zero, and the jump condition (2.30) implies that there is no flux  $\mathcal{F}^v$  of phase  $v$  across the boundary

$$\mathcal{F}^v = - \sum_{\forall \mu} S_{v\mu} \phi^v \phi^\mu + D_r \frac{\partial \phi^v}{\partial z} = 0, \quad \text{on } z = s(x, y, t), \quad (2.32)$$

where  $\phi_-^v = \phi^v$ . Exactly analogous boundary conditions for each of the phases hold at the base of the avalanche  $z = b(x, y)$ .

When there is no diffusion the boundary conditions (2.32) are considerably simplified. In most instances they are satisfied by setting either

$$\phi^v = 0 \quad \text{or} \quad \phi^v = 1, \quad \text{on } z = s, b. \quad (2.33)$$

The second condition works because it implies that  $\phi^\mu = 0$  for all  $\mu \neq v$  and hence that the sum  $\sum_{\forall \mu} S_{v\mu} \phi^\mu$  in (2.32) is zero. Note that the sum is equal to minus the velocity of phase  $v$  relative to the bulk,  $-(w^v - w)$ , by (2.25), so it is possible for it to be zero for concentrations in the range  $0 < \phi^\mu < 1$ . This usually implies that there is a net flux of both larger and smaller particles through the boundary, which violates the conditions placed on the other phases. It follows that in most instances the only realizable boundary condition is (2.33). The only time in which this is not the case is when there is a constituent that does not segregate with any of the other particles. An example in which this occurs is investigated in greater detail in § 10.

### 3. Segregation and remixing in two-component mixtures

It is useful to relate the multi-component theory to the familiar case of a two-component mixture of large and small particles. The two phases are referred to by the constituent letters  $v = l$  for large particles and  $v = s$  for small particles. The formula (2.27) implies that for two constituents ( $j = 2$ ) just one segregation coefficient must be specified, i.e. either  $S_{ls}$  or  $S_{sl} = -S_{ls}$ . In the absence of diffusion, (2.25) implies that

the normal components of the large and small velocities are given by

$$w^l = w + S_{ls}\phi^s, \quad (3.1)$$

$$w^s = w - S_{ls}\phi^l, \quad (3.2)$$

respectively. It follows that if  $S_{ls}$  is chosen to be positive, the large particles will rise relative to the bulk material until there are no more small particles, while the small particles will percolate downwards until there are no more large particles. This paper will adopt the convention of prescribing the positive segregation rates, which in this case is  $S_{ls}$ . The multi-component theory yields two segregation–remixing equations (2.28) for the large and small particles

$$\frac{\partial \phi^l}{\partial t} + \nabla \cdot (\phi^l \mathbf{u}) + \frac{\partial}{\partial z} (S_{ls} \phi^l \phi^s) = \frac{\partial}{\partial z} \left( D_r \frac{\partial \phi^l}{\partial z} \right), \quad (3.3)$$

$$\frac{\partial \phi^s}{\partial t} + \nabla \cdot (\phi^s \mathbf{u}) - \frac{\partial}{\partial z} (S_{ls} \phi^s \phi^l) = \frac{\partial}{\partial z} \left( D_r \frac{\partial \phi^s}{\partial z} \right). \quad (3.4)$$

The summation condition (2.3) implies that the particle concentrations are related by

$$\phi^l + \phi^s = 1, \quad (3.5)$$

and one of the variables in either (3.3) or (3.4) can be eliminated. Gray & Thornton (2005) and Gray & Chugunov (2006) both decided to substitute for the large particle concentration, which implies that the segregation–remixing equation for the concentration of the small particles becomes

$$\frac{\partial \phi^s}{\partial t} + \nabla \cdot (\phi^s \mathbf{u}) - \frac{\partial}{\partial z} (S_{ls} \phi^s (1 - \phi^s)) = \frac{\partial}{\partial z} \left( D_r \frac{\partial \phi^s}{\partial z} \right). \quad (3.6)$$

Dolgunin & Ukolov (1995) were the first to write down this equation, based on the simple insight that the segregation flux  $-S_{ls}\phi^s(1 - \phi^s)$  must shut off when there are either all small particles or all large ones. The equation is closely related to Burgers' equation, which Gray & Chugunov (2006) exploited to construct exact solutions for time-dependent segregation, by using the Cole–Hopf transformation (Hopf 1950; Cole 1951) to linearize both the segregation–remixing equation (3.6) and the boundary conditions (2.32). Khakhar *et al.* (1997) used the same equation to investigate particle density-driven segregation and found good agreement with experiments in rotating drums and with particle dynamics simulations.

Although the diffusive theory is able to model experiments and particle dynamics simulations more accurately, considerable insights have been gained from the non-diffusive version of the theory, which is much more amenable to analysis. This situation is reminiscent of shock waves in hydraulic and supersonic flows, in which sharp gradients in flow depth or density are replaced by shock waves (i.e. discontinuous solutions), which greatly simplifies the mathematical treatment. In the absence of diffusion, (3.6) can be written as

$$\frac{\partial \phi^s}{\partial t} + \frac{\partial}{\partial x} (\phi^s u) + \frac{\partial}{\partial y} (\phi^s v) + \frac{\partial}{\partial z} (\phi^s w) - \frac{\partial}{\partial z} (S_{ls} \phi^s (1 - \phi^s)) = 0, \quad (3.7)$$

which is a hyperbolic scalar conservation law. A steady-state two-dimensional version of this equation was first derived by Savage & Lun (1988) using information entropy theory, and Savage & Lun (1988) and Vallance & Savage (2000) showed that the solutions were consistent with their experiments on an inclined chute. The segregation equation (3.7) is closely related to the inviscid Burgers' equation, as well as models

of traffic flow (Whitham 1974) and the theory of sedimentation (Kynch 1952; Rhee, Aris & Amundson 1986). Using the incompressibility condition (2.29), (3.7) can be written in the quasi-linear form

$$\frac{\partial \phi^s}{\partial t} + u \frac{\partial \phi^s}{\partial x} + v \frac{\partial \phi^s}{\partial y} + w \frac{\partial \phi^s}{\partial z} + S_{ls}(2\phi^s - 1) \frac{\partial \phi^s}{\partial z} = 0, \quad (3.8)$$

which can be solved by the method of characteristics. A range of two-dimensional steady-state (Gray & Thornton 2005; Thornton *et al.* 2006) and time-dependent (Gray, Shearer & Thornton 2006; Shearer, Gray & Thornton 2008; Shearer & Dafermos 2010) exact solutions and proofs have been constructed. A highlight of the theory is its ability to predict the formation of breaking size segregation waves, which form whenever small particles are sheared over large ones (Thornton & Gray 2008; Gray & Ancey 2009; Shearer & Giffen 2010). The waves allow large and small particles to be recirculated in the flow, and are particularly important in the geophysical context, where they are fundamental to the formation of bouldery flow fronts (Gray & Ancey 2009; Gray & Kokelaar 2010*a, b*), lateral levees and digitate lobate terminations (Pierson 1986; Pouliquen *et al.* 1997; Pouliquen & Vallance 1999; Iverson & Vallance 2001; Félix & Thomas 2004; Goujon, Dalloz-Dubrujeaud & Thomas 2007; Cagnoli & Romano 2010; Iverson *et al.* 2010). A brief review of some of the recent results for both the bi-disperse diffusive and hyperbolic models can be found in Gray (2010).

#### 4. Segregation and remixing in three-component mixtures

Consider a three-constituent mixture of large, medium and small particles, which will be denoted by the constituent letters  $v = l, m, s$ . The formula (2.27) implies that for  $j = 3$  three segregation coefficients need to be specified. The convention that  $S_{v\mu}$  are positive can be satisfied by ensuring that constituent  $v$  is larger than constituent  $\mu$ . In this mixture the three independent segregation coefficients are  $S_{lm}$ ,  $S_{ls}$  and  $S_{ms}$ . The negative segregation coefficients  $S_{ml} = -S_{lm}$ ,  $S_{sl} = -S_{ls}$  and  $S_{sm} = -S_{ms}$  by the antisymmetric property of  $\mathbf{S}$ . It follows from (2.25) that in the absence of diffusion, the normal velocity of each constituent is

$$w^l = w + S_{lm}\phi^m + S_{ls}\phi^s, \quad (4.1)$$

$$w^m = w - S_{lm}\phi^l + S_{ms}\phi^s, \quad (4.2)$$

$$w^s = w - S_{ls}\phi^l - S_{ms}\phi^m. \quad (4.3)$$

These equations imply that, relative to the bulk flow, the large particles rise until there are no more small- or medium-sized particles, the small particles percolate downwards until there are no more large- or medium-sized particles, and the medium-sized particles may rise or fall depending on the local particle concentrations, and the segregation rates, until there are no more large or small particles surrounding them.

The multi-component segregation theory derived in § 2 now yields three segregation-remixing equations (2.28) for the concentrations of large, medium and small particles

$$\frac{\partial \phi^l}{\partial t} + \nabla \cdot (\phi^l \mathbf{u}) + \frac{\partial}{\partial z} (S_{lm}\phi^l\phi^m + S_{ls}\phi^l\phi^s) = \frac{\partial}{\partial z} \left( D_r \frac{\partial \phi^l}{\partial z} \right), \quad (4.4)$$

$$\frac{\partial \phi^m}{\partial t} + \nabla \cdot (\phi^m \mathbf{u}) + \frac{\partial}{\partial z} (-S_{lm}\phi^m\phi^l + S_{ms}\phi^m\phi^s) = \frac{\partial}{\partial z} \left( D_r \frac{\partial \phi^m}{\partial z} \right), \quad (4.5)$$

$$\frac{\partial \phi^s}{\partial t} + \nabla \cdot (\phi^s \mathbf{u}) + \frac{\partial}{\partial z} (-S_{ls}\phi^s\phi^l - S_{ms}\phi^s\phi^m) = \frac{\partial}{\partial z} \left( D_r \frac{\partial \phi^s}{\partial z} \right), \quad (4.6)$$



respectively. The summation condition (2.3) implies that

$$\phi^l + \phi^m + \phi^s = 1, \quad (4.7)$$

which allows one of the three equations (4.4)–(4.6) to be eliminated. For instance, substituting for  $\phi^m$  in (4.4) and (4.6) yields two coupled equations for the large and small particle concentrations,

$$\frac{\partial \phi^l}{\partial t} + \nabla \cdot (\phi^l \mathbf{u}) + \frac{\partial}{\partial z} (S_{lm} \phi^l (1 - \phi^l - \phi^s) + S_{ls} \phi^l \phi^s) = \frac{\partial}{\partial z} \left( D_r \frac{\partial \phi^l}{\partial z} \right), \quad (4.8)$$

$$\frac{\partial \phi^s}{\partial t} + \nabla \cdot (\phi^s \mathbf{u}) + \frac{\partial}{\partial z} (-S_{ls} \phi^s \phi^l - S_{ms} \phi^s (1 - \phi^l - \phi^s)) = \frac{\partial}{\partial z} \left( D_r \frac{\partial \phi^s}{\partial z} \right). \quad (4.9)$$

These are both very similar in form to the two-component segregation–remixing equation (3.6). In fact, if  $S_{ls} = S_{ms}$  the small particle concentration equation (4.9) degenerates to the two-component case. Standard numerical methods will be used to solve the coupled system of parabolic segregation–remixing equations in §§ 7, 9 and 10, but first some of the properties of the non-diffusive system will be examined.

## 5. Loss of hyperbolicity of the segregation equations

It is important to understand whether the system (4.4)–(4.6) is hyperbolic in the absence of diffusive terms. Using the incompressibility condition (2.29) the transport terms can be simplified just as in the case of the two-component mixture in § 3. Defining the material derivative

$$\frac{D}{Dt} = \frac{\partial}{\partial t} + \mathbf{u} \cdot \nabla, \quad (5.1)$$

the reduced system can be written in vector form as

$$\frac{D\boldsymbol{\phi}}{Dt} + \mathbf{A} \frac{\partial \boldsymbol{\phi}}{\partial z} = \mathbf{0}, \quad (5.2)$$

where the vector  $\boldsymbol{\phi} = (\phi^l, \phi^m, \phi^s)^T$ , the vector  $\mathbf{0} = (0, 0, 0)^T$  and the matrix of coefficients

$$\mathbf{A} = \begin{pmatrix} S_{lm}\phi^m + S_{ls}\phi^s & S_{lm}\phi^l & S_{ls}\phi^l \\ -S_{lm}\phi^m & -S_{lm}\phi^l + S_{ms}\phi^s & S_{ms}\phi^m \\ -S_{ls}\phi^s & -S_{ms}\phi^s & -S_{ls}\phi^l - S_{ms}\phi^m \end{pmatrix}. \quad (5.3)$$

This is equivalent to switching from an Eulerian to a Lagrangian frame. The characteristic wave speeds of the system (5.2) are calculated by finding the eigenvalues of the matrix  $\mathbf{A}$  (e.g. Lax 1957; Courant & Hilbert 1962; Joseph & Saut 1990). The characteristic determinant of the system is

$$\det(\mathbf{A} - \lambda \mathbf{I}) = 0, \quad (5.4)$$

where  $\mathbf{I}$  is the unit matrix. The trivial eigenvalue  $\lambda = 0$  is easily spotted and results from the fact that the segregation fluxes sum to zero over all constituents. The rows of the matrix  $\mathbf{A}$  are therefore linearly dependent. The trivial root is not important and in fact disappears in the system (4.8)–(4.9) in which  $\phi^m$  is eliminated. After dividing the trivial root out and substituting for  $\phi^m$  from (4.7), the characteristic determinant yields a quadratic equation for the wave speed  $\lambda$ ,

$$\lambda^2 + \gamma_1 \lambda + \gamma_2 = 0, \quad (5.5)$$

where the coefficients

$$\gamma_1 = (2S_{lm} - S_{ms} + S_{ls})\phi^l + (S_{lm} - 2S_{ms} - S_{ls})\phi^s + S_{ms} - S_{lm}, \quad (5.6)$$

$$\begin{aligned} \gamma_2 = & (2S_{lm}S_{ls} - 2S_{lm}S_{ms})(\phi^l)^2 - 4S_{lm}S_{ms}\phi^l\phi^s + (2S_{ls}S_{ms} - 2S_{lm}S_{ms})(\phi^s)^2 \\ & + (3S_{lm}S_{ms} - S_{lm}S_{ls})\phi^l + (3S_{lm}S_{ms} - S_{ls}S_{ms})\phi^s - S_{lm}S_{ms}. \end{aligned} \quad (5.7)$$

The two characteristic wave speeds in the Lagrangian frame are therefore

$$\lambda_{1,2} = \frac{-\gamma_1 \pm \sqrt{\gamma_1^2 - 4\gamma_2}}{2}. \quad (5.8)$$

The type of the system is determined by the discriminant  $\Delta = \gamma_1^2 - 4\gamma_2$ . If the discriminant is strictly positive,  $\Delta > 0$ , there are always two distinct real wave speeds  $\lambda_1$  and  $\lambda_2$  and the system is hyperbolic (e.g. Lax 1957; Courant & Hilbert 1962). If the discriminant is greater than or equal to zero,  $\Delta \geq 0$ , there can be a repeated root  $\lambda$ , and the equations are non-strictly hyperbolic. If, however,  $\Delta < 0$ , all the eigenvalues are complex and the system is elliptic (Joseph & Saut 1990). Such changes of type are not uncommon, occurring for instance in steady transonic flows. Joseph & Saut (1990) defined such problems to be of mixed type. However, elliptic initial-value problems are ill-posed, since the amplitude of small oscillations grows at an unbounded rate as their wavelength tends to zero. Such unbounded short-wavelength instabilities are known as Hadamard instabilities (e.g. Joseph & Saut 1990; Gray 1999; Goddard 2003) and are usually a sign that some important regularizing physics is missing in the model.

With some algebra it is possible to substitute the coefficients (5.6) and (5.7) into the discriminant  $\Delta$  and rearrange it into the reasonably compact form:

$$\begin{aligned} \Delta = & [(S_{ls} - 2S_{lm} - S_{ms})\phi^l + (S_{ls} - S_{lm} - 2S_{ms})\phi^s + S_{lm} + S_{ms}]^2 \\ & - 4(S_{ls} - S_{ms})(S_{ls} - S_{lm})\phi^l\phi^s. \end{aligned} \quad (5.9)$$

The discriminant is positive provided the segregation parameters lie in the domain

$$\Omega_1: \quad S_{ms} \geq S_{ls} \geq S_{lm}, \quad (5.10)$$

or in the domain

$$\Omega_2: \quad S_{lm} \geq S_{ls} \geq S_{ms}, \quad (5.11)$$

which were illustrated schematically in figure 4, using maximum segregation velocities  $q_{v\mu}$  instead of  $S_{v\mu}$ . It follows that the system of equations is non-strictly hyperbolic, for all mixture concentrations, provided the segregation parameters lie in  $\Omega_1 \cup \Omega_2$ . Note, that in the degenerate case,  $S_{ls} = S_{ms}$ , it is easy to use (5.9) to substitute back into (5.8) for the wave speed  $\lambda_2 = S_{ls}(2\phi^s - 1)$ , which is the same as that of the two-component model.

There are other regions of parameter space that are also non-strictly hyperbolic. Figure 5 shows a contour plot of the discriminant for an example in which both  $S_{lm}$  and  $S_{ms}$  are less than  $S_{ls}$ . In the unshaded region the discriminant is positive, but in the shaded region it can be negative. Fortunately, the shaded region also corresponds to combinations of concentrations that are not admissible. This is because for a given value of the small particle concentration  $\phi^s \in [0, 1]$ , the large particle concentration must lie in the range  $0 \leq \phi^l \leq 1 - \phi^s$ , so all the valid concentrations must lie below the line  $\phi^l = 1 - \phi^s$ . For the particular choice of segregation parameters used in figure 5, the discriminant  $\Delta$  is greater than or equal to zero and the equations are therefore non-strictly hyperbolic. In order to extend this idea, it is useful to be able to move

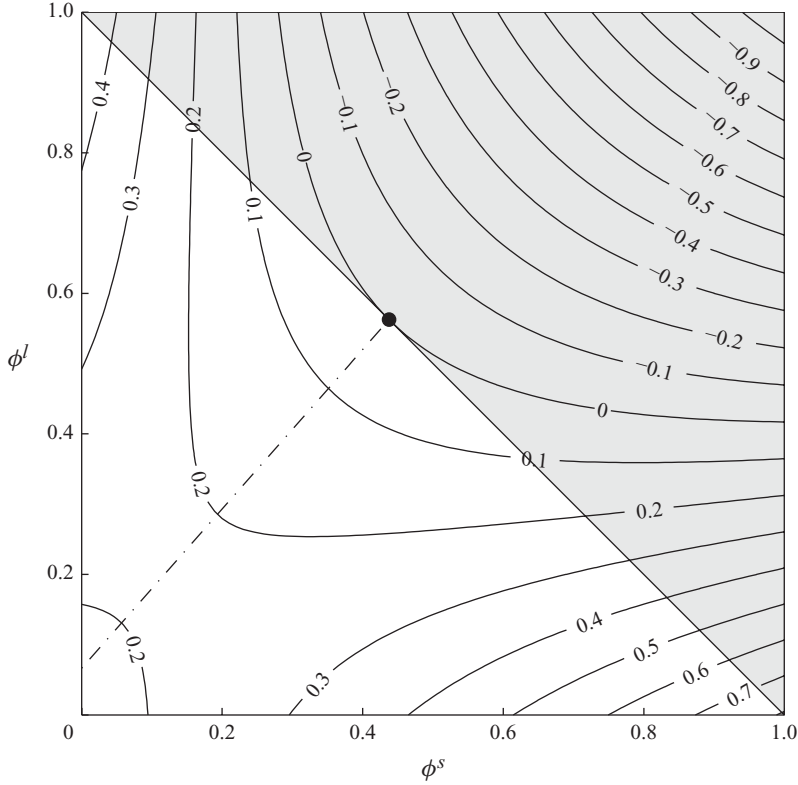


FIGURE 5. A contour plot of the discriminant  $\Delta$  as a function of the large and small particle concentrations,  $\phi^l$  and  $\phi^s$ , for segregation parameters  $S_{ls} = 1$ ,  $S_{lm} = 3/10$  and  $S_{ms} = 1/10$ . For a given value of  $\phi^s$ , the large particle concentration must lie in the range of  $\phi^l \in [0, 1 - \phi^s]$ . The grey-shaded region indicates the concentration combinations that are not admissible. Moving in parameter space along lines parallel to  $\phi^l = 1 - \phi^s$ , the discriminant has a local minimum along the dot-dashed line. The global minimum equals zero and is attained at the black dot, where the zero contour touches the  $\phi^l = 1 - \phi^s$  line.

through the concentration space without entering the grey-shaded region. This can be done by defining a new variable  $\delta \in [0, 1]$  that parameterizes a series of lines that lie parallel to  $\phi^l = 1 - \phi^s$ , by letting

$$\phi^l = \delta - \phi^s. \quad (5.12)$$

Substituting (5.12) into (5.9) yields an alternative quadratic representation of the discriminant

$$\Delta = \gamma_3(\phi^s)^2 + \gamma_4\phi^s + \gamma_5, \quad (5.13)$$

where some of the coefficients are now dependent on  $\delta$ :

$$\gamma_3 = (S_{lm} + S_{ms} - 2S_{ls})^2, \quad (5.14)$$

$$\gamma_4 = 2(S_{ls}S_{ms} + 3S_{lm}S_{ls} - S_{lm}S_{ms} - 2S_{ls}^2 - 2S_{lm}^2 + S_{ms}^2)\delta + 2S_{lm}^2 - 2S_{ms}^2, \quad (5.15)$$

$$\gamma_5 = ((S_{ms} + 2S_{lm} - S_{ls})\delta - S_{lm} - S_{ms})^2. \quad (5.16)$$

Restricting ourselves to regions of parameter space outside  $\Omega_1 \cup \Omega_2$ , the coefficient  $\gamma_3$  is strictly positive and the quadratic (5.13) has a local minimum for each value of the parameter  $\delta$ . The small particle concentration and the discriminant, at the local

minimum, can therefore be defined as functions of  $\delta$  by

$$\phi_{min}^s(\delta) = -\frac{\gamma_4}{2\gamma_3} \quad \text{and} \quad \Delta_{min}(\delta) = \gamma_5 - \frac{\gamma_4^2}{4\gamma_3}, \quad (5.17)$$

respectively. In concentration space the local minima lie on the curve  $(\phi_{min}^s(\delta), \delta - \phi_{min}^s(\delta))$ , which corresponds to the dot-dashed line in figure 5. Substituting for the coefficients  $\gamma_3$ ,  $\gamma_4$  and  $\gamma_5$  the discriminant at the local minimum becomes

$$\Delta_{min}(\delta) = \gamma_6(S_{ls} - S_{ms})(S_{ls} - S_{lm}) [(S_{lm} + S_{ms})(1 - \delta) + (2S_{ls} - S_{lm} - S_{ms})\delta], \quad (5.18)$$

where the constant

$$\gamma_6 = \frac{4(1 - \delta)(S_{lm} + S_{ms})}{(S_{lm} + S_{ms} - 2S_{ls})^2} \quad (5.19)$$

is positive. Rather interestingly, (5.18) and (5.19) imply that the discriminant equals zero when  $\delta$  is equal to unity. There will therefore always be a point on the line  $\phi^l = 1 - \phi^s$  where the discriminant is zero. This point is indicated by the black dot in figure 5. In the domain

$$\Omega_3: \quad S_{ls} > S_{lm} \quad \text{and} \quad S_{ls} > S_{ms}, \quad (5.20)$$

(5.18) shows that  $\Delta_{min}$  is positive for all admissible concentrations. The discriminant  $\Delta \geq \Delta_{min}$  is therefore positive and the system is non-strictly hyperbolic in  $\Omega_3$  for all admissible concentrations.

This leaves the region

$$\Omega_4: \quad S_{ls} < S_{lm} \quad \text{and} \quad S_{ls} < S_{ms}, \quad (5.21)$$

where  $\Delta_{min}$  can be positive or negative. It follows that the discriminant  $\Delta \geq \Delta_{min}$  can be positive or negative and hence that the system is either hyperbolic or elliptic, depending on the local concentrations and the segregation parameters. An example of this, for segregation parameters  $S_{ls} = 1/8$ ,  $S_{lm} = 1$  and  $S_{ms} = 3/8$ , is shown in figure 6. The region of negative discriminant, and hence where the system is elliptic, lies within the zero contour, which is elliptical in shape and tangent to the  $\phi^l$  and  $\phi^s$  axes as well as the line  $\phi^l = 1 - \phi^s$ . Outside the region the equations are non-strictly hyperbolic. Even if the problem is initially hyperbolic everywhere, the system may change its type as the concentrations evolve, to create regions of ellipticity. Since the regions of ellipticity occur in a time-dependent problem, this necessarily leads to short-wavelength Hadamard instabilities and ill-posedness (e.g. Joseph & Saut 1990; Gray 1999; Goddard 2003). In order to guarantee non-strict hyperbolicity, for all admissible concentrations, it is necessary to restrict the segregation model to parameter ranges that lie in the union of  $\Omega_1$ ,  $\Omega_2$  and  $\Omega_3$ . Solutions for particular cases may also exist in region  $\Omega_4$ , but they cannot be guaranteed.

## 6. Regularization by diffusive remixing

Golick & Daniels (2009) used their annular shear cell to measure the time scale  $t_s$  for complete segregation to occur, as a function of grain-size ratio, and found that there was a minimum at a grain-size ratio of 2. This suggests that the graph of the maximum segregation velocity,  $q_{v\mu}$ , as a function of grain-size ratio  $r_v/r_\mu$ , should have a maximum at  $r_v/r_\mu = 2$ , as illustrated in figure 4(a). If this is the case then, in a ternary mixture, it is possible to choose the grain-size ratios so that the largest and smallest grains segregate more slowly from each other, than each of them do with

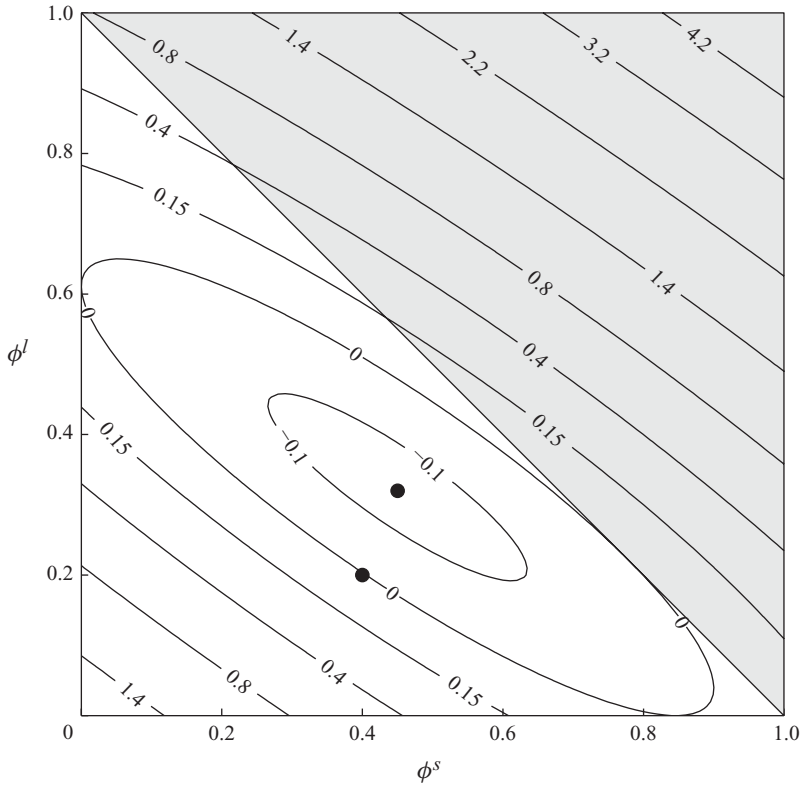


FIGURE 6. A contour plot of the discriminant  $\Delta$  as a function of the large and small particle concentrations,  $\phi^l$  and  $\phi^s$ , for segregation parameters  $S_{ls} = 1/8$ ,  $S_{lm} = 1$  and  $S_{ms} = 3/8$ . The discriminant is negative in the elliptical region inside the zero contour. The grey-shaded region indicates the concentration combinations that are not admissible and the markers indicate the initial conditions for which simulations have been performed.

the medium-sized grains. The segregation parameters can therefore lie in domain  $\Omega_4$ , defined in (5.21) and illustrated in figure 4(d), where the non-diffusive segregation theory can break down. In this section, it is shown that the effects of diffusive remixing are sufficient to completely suppress the short-wavelength Hadamard instability in  $\Omega_4$  and hence regularize the model, making it applicable over all domains of parameter space. Consider the simplified problem in which the grains are initially homogeneously distributed throughout the avalanche,

$$\phi^v(x, z, 0) = \phi_0^v. \quad (6.1)$$

For this initial condition no downstream or cross-stream gradients in concentration develop. It follows that the large and small particle segregation-remixing equations (4.8)–(4.9) reduce to

$$\frac{\partial \phi^l}{\partial t} = \frac{\partial}{\partial z} \left( -S_{lm} \phi^l (1 - \phi^l - \phi^s) - S_{ls} \phi^l \phi^s + D_r \frac{\partial \phi^l}{\partial z} \right), \quad (6.2)$$

$$\frac{\partial \phi^s}{\partial t} = \frac{\partial}{\partial z} \left( S_{ls} \phi^s \phi^l + S_{ms} \phi^s (1 - \phi^l - \phi^s) + D_r \frac{\partial \phi^s}{\partial z} \right). \quad (6.3)$$



Away from the boundaries, the constant initial concentration (6.1) is a solution of the system. Linearizing (6.2)–(6.3) about the initial state by substituting

$$\phi^v = \phi_0^v + \phi_*^v, \quad (6.4)$$

where  $\phi_*^v$  is a small perturbation, implies that

$$\frac{\partial \phi_*^l}{\partial t} = a_{11} \frac{\partial \phi_*^l}{\partial z} + a_{12} \frac{\partial \phi_*^s}{\partial z} + D_r \frac{\partial^2 \phi_*^l}{\partial z^2}, \quad (6.5)$$

$$\frac{\partial \phi_*^s}{\partial t} = a_{21} \frac{\partial \phi_*^l}{\partial z} + a_{22} \frac{\partial \phi_*^s}{\partial z} + D_r \frac{\partial^2 \phi_*^s}{\partial z^2}, \quad (6.6)$$

where the matrix of coefficients

$$\mathbf{a} = \begin{pmatrix} -S_{lm} + 2S_{lm}\phi_0^l + S_{lm}\phi_0^s - S_{ls}\phi_0^s & (S_{lm} - S_{ls})\phi_0^l \\ (S_{ls} - S_{ms})\phi_0^s & S_{ls}\phi_0^l + S_{ms} - S_{ms}\phi_0^l - 2S_{ms}\phi_0^s \end{pmatrix}. \quad (6.7)$$

The system of equations (6.5)–(6.6) admits normal-mode solutions of the form

$$\phi_*^l = C_1 \exp(ikz + \omega t), \quad \phi_*^s = C_2 \exp(ikz + \omega t), \quad (6.8)$$

where  $k$  is the wavenumber,  $\omega$  is the growth rate and  $C_1$  and  $C_2$  are constant coefficients. Substituting the normal modes into (6.5)–(6.6) yields a matrix eigenvalue problem

$$\begin{pmatrix} -w + ika_{11} - D_r k^2 & ika_{12} \\ ika_{21} & -w + ika_{22} - D_r k^2 \end{pmatrix} \begin{pmatrix} C_1 \\ C_2 \end{pmatrix} = \begin{pmatrix} 0 \\ 0 \end{pmatrix}, \quad (6.9)$$

which has non-trivial solutions when the determinant of the matrix is zero. Solving the resulting quadratic equation implies that the growth rates are

$$\omega_{1,2} = \left( -D_r k + \frac{i}{2}a_{11} + \frac{i}{2}a_{22} \pm \frac{i}{2}\sqrt{(a_{22} - a_{11})^2 + 4a_{21}a_{12}} \right) k. \quad (6.10)$$

The term inside the square root is independent of diffusion. Moreover, by comparing the coefficients of the matrix  $\mathbf{a}$  and the definition of the characteristic discriminant in (5.9) it is easy to see that the term inside the square root is the discriminant  $\Delta$  evaluated at the initial concentration, i.e.  $\Delta_0 = (a_{22} - a_{11})^2 + 4a_{21}a_{12}$ . It follows that (6.10) can also be written as

$$\omega_{1,2} = \left( -D_r k + \frac{i}{2}a_{11} + \frac{i}{2}a_{22} \pm \frac{i}{2}\sqrt{\Delta_0} \right) k. \quad (6.11)$$

The initial condition is stable if the real part of the growth rate is negative, it is neutrally stable when the real part is zero, and when the real part is positive the initial state is linearly unstable. The largest real root of (6.11) is simply

$$\text{Re}(\omega_1) = \begin{cases} -D_r k^2, & \Delta_0 \geq 0, \\ -D_r k^2 + \frac{k}{2}\sqrt{-\Delta_0}, & \Delta_0 < 0. \end{cases} \quad (6.12)$$

It follows immediately from our analysis of the segregation model that, provided the diffusion  $D_r$  is non-zero, the initial condition is stable for segregation parameters in the domains  $\Omega_1$ ,  $\Omega_2$  and  $\Omega_3$ , since the discriminant is positive and the growth rate is negative. When  $D_r$  is equal to zero the system is neutrally stable. In domain  $\Omega_4$  the situation is more complex as the discriminant can either be positive, negative or zero,

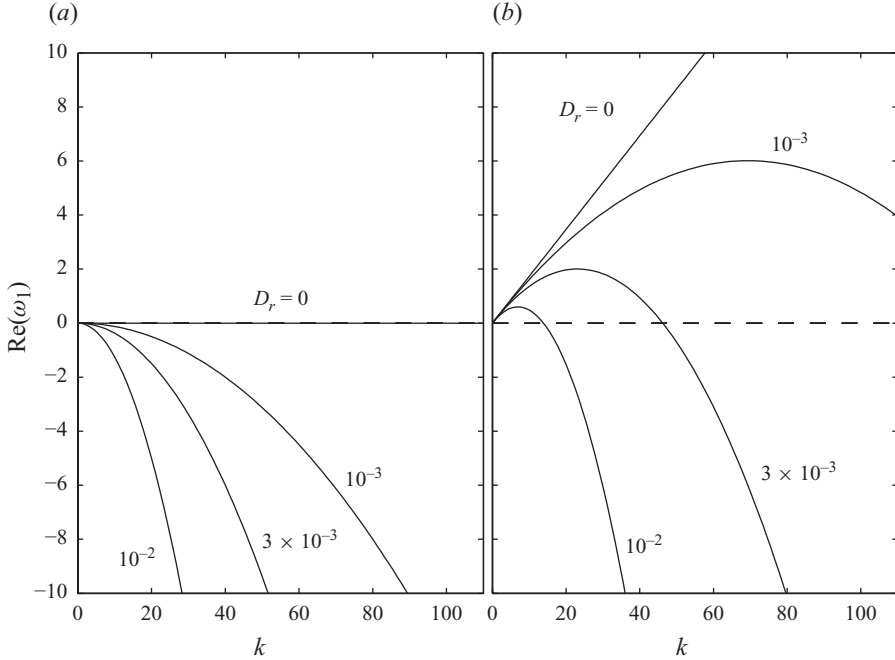


FIGURE 7. Two plots of the real part of the growth rate  $\omega_1$  as a function of the wavenumber  $k$  for four different diffusion rates  $D_r = 0, 10^{-3}, 3 \times 10^{-3}$  and  $10^{-2}$ . Both sets of plots are for  $S_{ls} = 1/8$ ,  $S_{lm} = 1$  and  $S_{ms} = 3/8$ . Plot (a) is for concentration  $\phi_0^l = 0.2$  and  $\phi_0^s = 0.4$  and plot (b) is for  $\phi_0^l = 0.32$  and  $\phi_0^s = 0.45$ , which correspond to the states represented by the two markers in figure 6.

so the initial state can be linearly unstable, stable or neutrally stable, depending on whether it lies inside, outside or on the elliptical zero contour line illustrated in figure 6. The largest growth rate is plotted for two states in figure 7. The first state, shown in figure 7(a), lies just outside the elliptical region and is linearly stable for all non-zero diffusion coefficients, while the second state lies close to the centre of the elliptical region, and has a region of unstable wavenumbers for all values of the diffusion coefficient, as shown in figure 7(b). This region of instability becomes progressively smaller, as does the magnitude of the growth, as the diffusion coefficient  $D_r$  increases. Most importantly,  $\text{Re}(\omega_1) \rightarrow -D_r k^2$  as  $k \rightarrow \infty$  provided  $D_r > 0$ , which implies that large wavenumber perturbations are damped out. When  $D_r = 0$ , the growth rate  $\text{Re}(\omega_1) \rightarrow k\sqrt{-\Delta_0}/2$ , which is unbounded as  $k \rightarrow \infty$ , and proves that the non-diffusive model is Hadamard unstable and ill-posed in this region (Joseph & Saut 1990; Goddard 2003). In conclusion, diffusive remixing regularizes the segregation equations in domain  $\Omega_4$  and ensures that the segregation–remixing equations can be applied in all regions of parameter space.

## 7. Linearly stable and unstable time-dependent solutions

For certain initial concentrations within  $\Omega_4$ , the regularized system of segregation–remixing equations (6.2)–(6.3) is linearly unstable over a finite range of wavenumbers, and it is of interest to see how this linear instability manifests itself in practical situations. The parabolic time-dependent equations (6.2)–(6.3) are therefore solved numerically using a standard Galerkin finite element method (e.g Skeel & Berzins

1990), which is implemented in the `pdepe` routine contained in Matlab. An example Matlab script for the slightly more general two-dimensional steady-state problem, discussed in §9, can be found in the supplementary material. The time-dependent simulations in this paper were performed with a 400 point grid in  $z$ , using a relative error tolerance of  $10^{-6}$ .

The avalanche is assumed to be of unit depth and the boundary conditions at the surface and base of the flow are given by the no-flux condition (2.32). A small sinusoidal perturbation of amplitude 0.01 is given to the initially homogeneous concentration distribution

$$\phi^l(z, 0) = \phi_0^l + 0.01 \sin(2\pi n z), \quad 0 \leq z \leq 1, \quad (7.1)$$

$$\phi^s(z, 0) = \phi_0^s - 0.01 \sin(2\pi n z), \quad 0 \leq z \leq 1, \quad (7.2)$$

where  $n = 10$ . The system is then integrated forward in time to compute the concentrations of large and small particles  $\phi^l(x, z)$  and  $\phi^s(x, z)$ , and the concentration of medium-sized particles is then calculated from the summation condition (4.7).

Figure 8 shows the results for the linearly stable initial condition shown in figure 7(a), where the homogeneous concentrations are  $\phi_0^l = 0.2$  and  $\phi_0^s = 0.4$ . The diffusive remixing coefficient  $D_r = 10^{-3}$  is very small, so the solution, which is represented by a grey scale, has very sharp concentration gradients between regions of almost constant concentration. The initial sinusoidal disturbance is damped out, as predicted by the linear-stability analysis. As time increases, the grains sort themselves out into inversely graded layers with the large particles on top, the small particles at the bottom and the medium-sized grains in between, as shown in figure 8(a–c) as well as the concentration profiles at  $t = 6$  along the bottom. This one-dimensional time-dependent problem is closely related to two-dimensional steady-state segregation problems in the absence of velocity shear, with time  $t$  replacing the downslope coordinate  $x$ . Such segregation problems, both with and without shear, will be solved exactly in §8 and are easily adapted to the spatially uniform time-dependent case here. They show that the solution consists of six regions of constant concentration that are separated by eight linear concentration shocks. The discontinuities are illustrated by the straight solid lines in figure 8, which coincide with high concentration gradients in the diffuse case. The low diffusion limit is therefore well approximated by the hyperbolic segregation equations provided that the solution is linearly stable throughout its evolution.

In the linearly unstable region of parameter space, corresponding to the homogeneous initial condition  $\phi_0^l = 0.32$  and  $\phi_0^s = 0.45$ , shown in figure 7(b), the situation is rather different. This time the initial perturbations rapidly grow to form a series of stripes as shown in figure 9. The stripes strongly reflect the wavelength of the initial disturbance. This wavelength was chosen to be close to the maximum growth rate for a diffusion coefficient  $D_r = 10^{-3}$ . This was done in order to see evidence of the instability before it is annihilated by the regions of large and small grains, that collect at the surface and base of avalanche, due to the no-flux boundary conditions. The concentration profiles through the depth of the avalanche at  $t = 1.5$  show that the stripes have an interlocking comb-like, or sawtooth-like, structure. The strongest striping is in the concentration of the medium-sized grains. For these initial conditions, the phase speed  $-(a_{11} + a_{22})/2$  of the linear instability in §6 is almost identically zero. The stripes are therefore nearly parallel to the downslope direction. For other initial conditions, within the linearly unstable elliptic region shown in figure 6, the phase speed is considerably larger and the stripes can drift either upwards or downwards

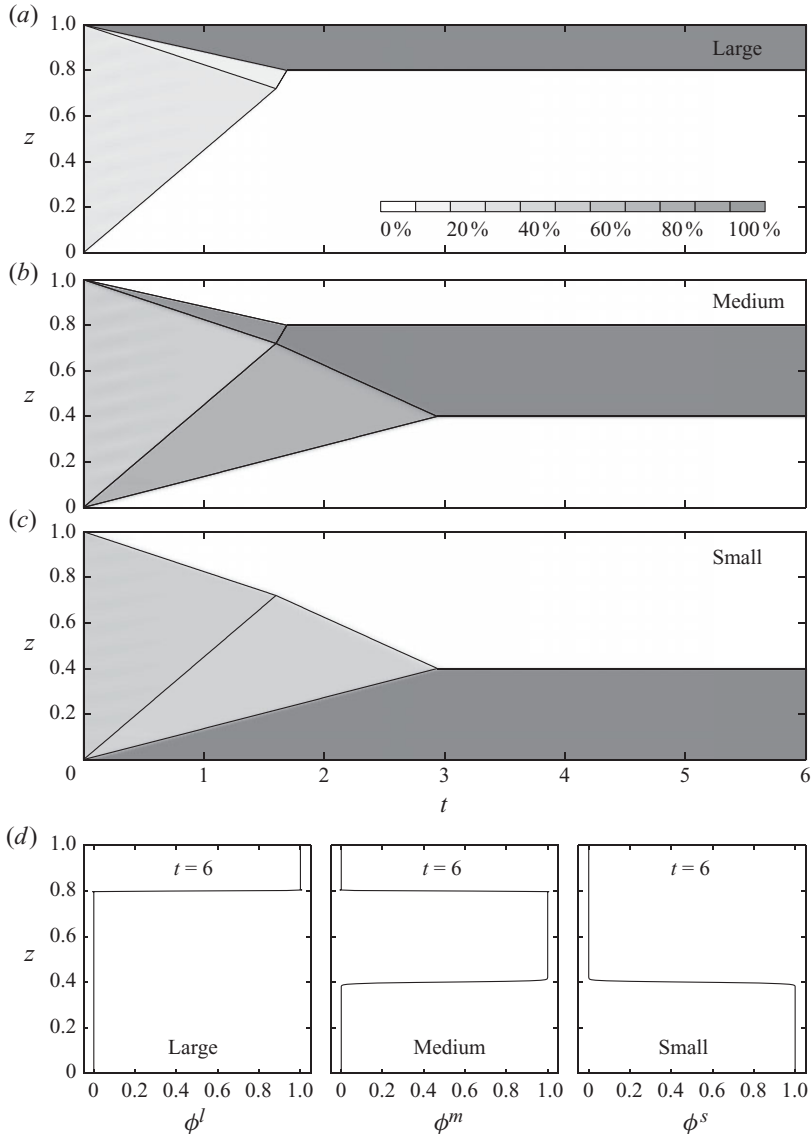


FIGURE 8. In (a–c) are shaded contour plots in  $(t, z)$  of the time-dependent evolution of the concentration of large, medium and small particles. The segregation parameters  $S_{ls} = 1/8$ ,  $S_{lm} = 1$  and  $S_{ms} = 3/8$ , the diffusive remixing coefficient  $D_r = 10^{-3}$ , and there is a small sinusoidal perturbation to inflow concentrations  $\phi_0^l = 0.2$ ,  $\phi_0^m = 0.4$  and  $\phi_0^s = 0.4$ . The plots use 64 grey levels and a scale with 11 levels is shown in (a). The solid lines show the position of concentration shocks, which have been adapted to the time-dependent case from the exact solution derived in §8. In (d), the final concentration profile at  $t=6$  is plotted for the large, medium and small particles.

as time progresses. Within the stripes, an individual large particle will still move upwards, but it will not rise at a constant rate, as in the linearly stable homogeneous case, but will speed up and slow down as it goes. Similarly, small particles do not percolate downwards at a constant rate. In this example, medium-sized particles have a tendency to percolate downwards, but as the stripes become stronger they

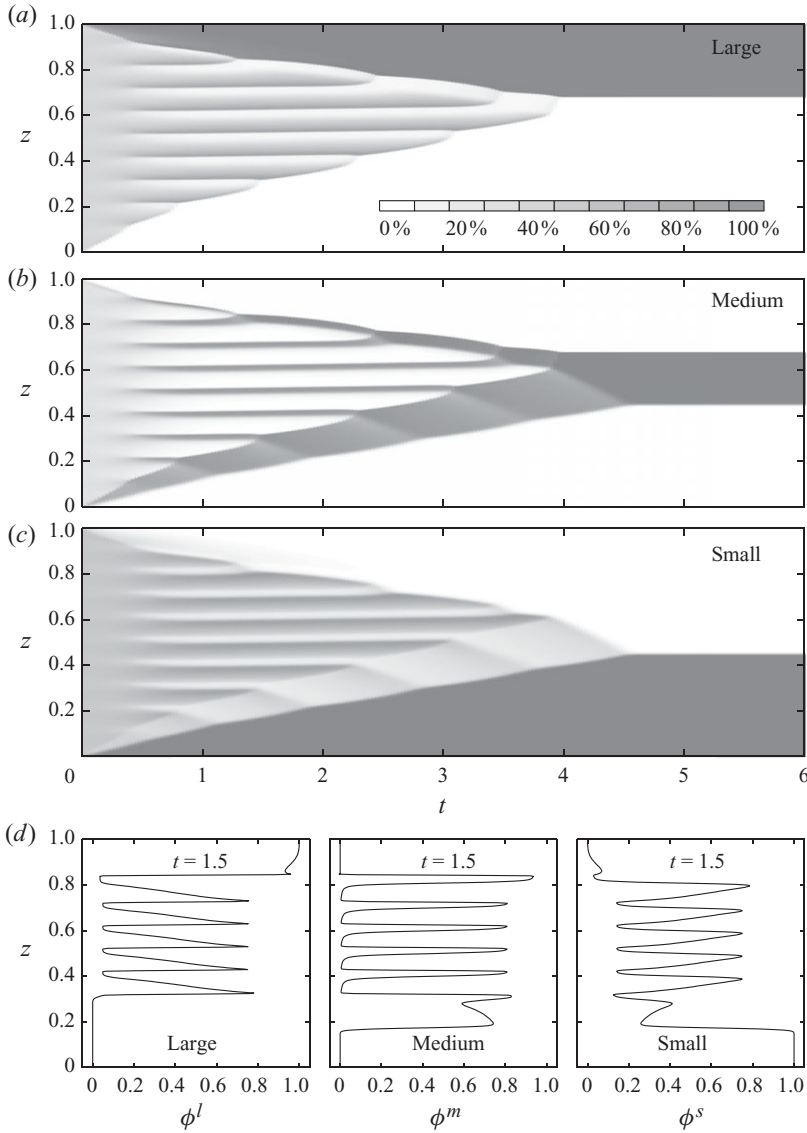


FIGURE 9. In (a–c) are shaded contour plots in  $(t, z)$  of the time-dependent evolution of the concentration of large, medium and small particles. The segregation parameters  $S_{ls} = 1/8$ ,  $S_{lm} = 1$  and  $S_{ms} = 3/8$ , the diffusive remixing coefficient  $D_r = 10^{-3}$ , and there is a small sinusoidal perturbation to inflow concentrations  $\phi_0^l = 0.32$ ,  $\phi_0^m = 0.23$  and  $\phi_0^s = 0.45$ . The plots use 64 grey levels and a scale with 11 levels is shown in (a). In (d), the concentration profile at  $t = 1.5$  is plotted for the large, medium and small particles.

get locked in and are concentrated still further. The triangular space–time region where the stripes occur has only a finite duration, and eventually the medium and small particles separate out into an almost bi-disperse phase, which is linearly stable, and the strong perturbations are then dissipated by segregation and diffusion. For sufficiently long time, the final state also approaches an inversely graded state with high concentrations of large at the top, high concentrations of fines at the bottom and the medium-sized grains in between.

## 8. Shock solutions for distribution grading in a ternary mixture

The time-dependent numerical solution in figure 8 shows that when the diffusive remixing coefficient  $D_r$  is relatively small, the segregation from a homogeneous initial state may reasonably be described by regions of constant concentration that are separated by jumps or shocks. In this section, the exact solution in the absence of diffusion is derived for a closely related steady two-dimensional problem.

### 8.1. Problem formulation

Savage & Lun (1988) and Gray & Thornton (2005) investigated the steady spatially evolving segregation of a bi-disperse mixture as it flowed down an inclined chute from a homogeneously mixed inflow condition. The avalanche was assumed to be of constant depth and the downslope velocity profile with depth  $u(z)$  was prescribed. The solutions have a relatively simple structure with regions of constant concentration separated by discontinuities. It is of considerable interest to investigate an analogous problem for a ternary mixture of large, medium and small particles. By virtue of the scalings (2.24), the avalanche is assumed, without loss of generality, to be of unit depth,  $h = 1$ , and has unit depth-averaged velocity,  $\bar{u} = 1$ . Assuming that the inflow lies at  $x = 0$ , the bulk velocity components are of the form

$$u(z) \geq 0, \quad v = 0, \quad w = 0 \quad \text{in } 0 \leq z \leq 1, \quad x \geq 0, \quad (8.1)$$

where the downslope velocity component has a monotonic profile with increasing  $z$ . The summation condition (2.3) implies that

$$\phi^l + \phi^m + \phi^s = 1, \quad (8.2)$$

which can be used to eliminate the concentration of medium particles in the large and small particle segregation equations (2.28). In the flow field (8.1) and in the absence of diffusion, these reduce to

$$u \frac{\partial \phi^l}{\partial x} + \frac{\partial}{\partial z} (S_{lm} \phi^l (1 - \phi^l - \phi^s) + S_{ls} \phi^l \phi^s) = 0, \quad (8.3)$$

$$u \frac{\partial \phi^s}{\partial x} + \frac{\partial}{\partial z} (-S_{ls} \phi^s \phi^l - S_{ms} \phi^s (1 - \phi^l - \phi^s)) = 0, \quad (8.4)$$

and the normal velocity (2.25) of each of the constituents becomes

$$w^l = S_{lm} \phi^m + S_{ls} \phi^s, \quad (8.5)$$

$$w^m = -S_{lm} \phi^l + S_{ms} \phi^s, \quad (8.6)$$

$$w^s = -S_{ls} \phi^l - S_{ms} \phi^m. \quad (8.7)$$

Note that the steady two-dimensional homogeneous inflow problem considered here is closely related to the time-dependent spatially uniform problem discussed in § 7. Indeed, in the absence of diffusion they are the same if  $(x, z)$  is mapped to  $(t, z)$  and the downstream velocity is assumed to be plug-like, i.e.  $u = 1$ .

At the inflow, the concentration of large and small particles is homogeneous through the depth of the avalanche

$$\phi^l(0, z) = \phi_0^l, \quad \phi^s(0, z) = \phi_0^s, \quad 0 \leq z \leq 1, \quad (8.8)$$

where  $\phi_0^l$  and  $\phi_0^s$  are constants. This necessarily implies that the concentration of medium-sized particles at the inflow is

$$\phi^m(0, z) = 1 - \phi_0^l - \phi_0^s = \phi_0^m, \quad 0 \leq z \leq 1, \quad (8.9)$$

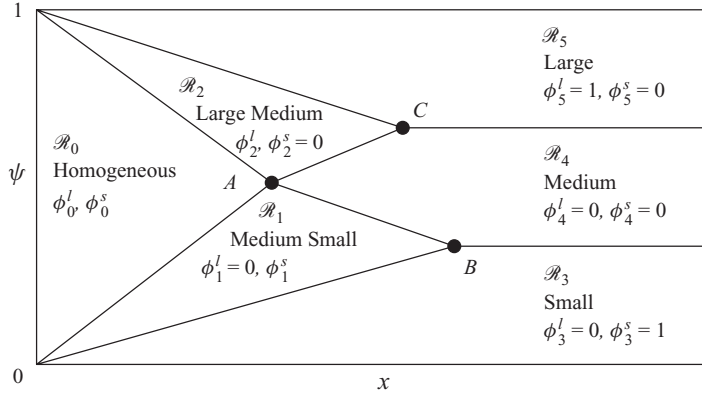


FIGURE 10. A sketch of the structure of the shock solution in  $(x, \psi)$ -mapped coordinates for distribution grading. The inflow is on the left where the large, medium and small particles enter in a homogeneously mixed state. Sufficiently far downstream the particles separate into inversely graded layers with the largest at the top, the smallest at the bottom and the medium-sized grains sandwiched in between. The solution consists of a series of shocks that separate regions  $\mathcal{R}_0$ – $\mathcal{R}_5$  of constant concentration. The subscripts  $i = 0$ – $5$  are used to identify the concentration  $\phi_i^\nu$  of particles  $\nu$  in each region. The points  $A$ ,  $B$  and  $C$  mark key points where the shocks intersect.

by (8.2). Sufficiently far downstream, the particles segregate out into inversely graded layers, with the largest grains at the top, the smallest particles at the bottom and the medium-sized ones in a layer between the two. This suggests that a solution exists with the shock structure shown in figure 10. The shocks are shown with straight line segments and in the regions  $\mathcal{R}_0$ – $\mathcal{R}_5$  that they enclose, the concentrations of large, medium and small particles are constant. The subscripts  $i = 0$ – $5$  are used to identify the constant concentration  $\phi_i^\nu$  of particles of phase  $\nu$  in each of the regions  $\mathcal{R}_0$ – $\mathcal{R}_5$  and the letters  $A$ ,  $B$  and  $C$  identify key shock intersections.

The position of the shocks and the magnitude of the discontinuities are controlled by the jump conditions (2.30). In the case where there is no diffusion,  $D_r = 0$ , and the shock, which lies at height  $z = z_{shock}(x)$ , does not propagate ( $v_n = 0$ ), the jump conditions for the large and small particles reduce to

$$[[\phi^l]]u \frac{d}{dx}(z_{shock}) = [[S_{lm}\phi^l\phi^m + S_{ls}\phi^l\phi^s]], \quad (8.10)$$

$$[[\phi^s]]u \frac{d}{dx}(z_{shock}) = [[-S_{ls}\phi^s\phi^l - S_{ms}\phi^s\phi^m]], \quad (8.11)$$

respectively. The jump condition for the medium-sized particles is a linear combination of (8.10) and (8.11) and does not provide any additional information. The problem is considerably simplified by working in depth-averaged velocity, or streamfunction, coordinates (Gray & Thornton 2005; Gray & Ancy 2009) defined by the integral

$$\psi = \int_0^{z_{shock}} u(z') dz'. \quad (8.12)$$

The base of the avalanche therefore lies at  $\psi = 0$  and, since  $\bar{u} = 1$ , the free surface lies at  $\psi = 1$  in the mapped coordinate system. Taking the derivative of  $\psi$  with respect to  $x$  implies  $d\psi/dx = u dz_{shock}/dx$  by Leibniz's integral theorem (see § 3.3.7, Abramowitz & Stegun 1970). It follows that in  $(x, \psi)$  coordinates, the jump conditions (8.10)–(8.11)

become

$$[[\phi^l]] \frac{d\psi}{dx} = [[S_{lm}\phi^l\phi^m + S_{ls}\phi^l\phi^s]], \quad (8.13)$$

$$[[\phi^s]] \frac{d\psi}{dx} = [[-S_{ls}\phi^s\phi^l - S_{ms}\phi^s\phi^m]], \quad (8.14)$$

which are independent of the velocity profile  $u(z)$ . Solutions can therefore be constructed in  $(x, \psi)$  coordinates for arbitrary downstream velocity fields and then mapped back to physical  $(x, z)$  space for specific cases.

### 8.2. Surface and basal double-shock structure

As the homogeneous mixture is swept downstream, the particles segregate relative to one another, with the large ones moving up, the small ones moving down and the medium-sized ones moving up or down depending on the local concentration. Within the bulk of the avalanche, the mixture stays at its initial inflow concentrations  $\phi_0^l$ ,  $\phi_0^m$  and  $\phi_0^s$ . However, at the base, the boundary conditions (2.33) imply that there is no further supply of large- or medium-sized particles. Assuming that the large particles rise fastest in the homogeneous mixture, the medium and small particles will separate out across a concentration shock. This is shown by the line segment  $OA$  in figure 10. Since there are no large particles on the forward side of the shock ( $\phi_1^l = 0$ ), the large particle jump condition (8.13) reduces to the ordinary differential equation

$$\frac{d\psi}{dx} = S_{lm}\phi_0^m + S_{ls}\phi_0^s = w_0^l, \quad (8.15)$$

where (8.5) implies that the right-hand side is equal to the normal velocity of the large particles  $w_0^l$  in the homogeneous mixture. This identification is important and will be used later. The concentrations  $\phi_0^m$  and  $\phi_0^s$  are known constants, and, provided that the segregation rates are constant, this can be integrated subject to the boundary condition that the shock starts at the base of the inflow,  $\psi(0) = 0$ , to give the line

$$\psi_{0A} = (S_{lm}\phi_0^m + S_{ls}\phi_0^s)x. \quad (8.16)$$

The subscript  $0A$  is used to identify it. The small particle jump condition (8.14) reduces to the ordinary differential equation

$$(\phi_1^s - \phi_0^s) \frac{d\psi}{dx} = -S_{ls}(\phi_1^s\phi_1^l - \phi_0^s\phi_0^l) - S_{ms}(\phi_1^s\phi_1^m - \phi_0^s\phi_0^m), \quad (8.17)$$

where  $\phi_1^m = 1 - \phi_1^s$  since  $\phi_1^l = 0$  as shown in figure 10. In this equation, the gradient  $d\psi/dx$  is known and can be substituted from (8.15) to obtain a quadratic equation for the small particle concentration  $\phi_1^s$  in the region  $\mathcal{R}_1$ ,

$$S_{ms}(\phi_1^s)^2 - (S_{lm}\phi_0^m + S_{ls}\phi_0^s + S_{ms})\phi_1^s + (S_{lm}\phi_0^m + S_{ls}(1 - \phi_0^m) + S_{ms}\phi_0^m)\phi_0^s = 0. \quad (8.18)$$

The shock conditions therefore determine both the position of the shock  $OA$  and the concentrations of the small- and medium-sized particles,  $\phi_1^s$  and  $\phi_1^m$ .

Within  $\mathcal{R}_1$  the medium-sized particles rise up and the small particles percolate downwards, except near the basal boundary  $OB$  where there is no further supply of medium-sized particles, and the small ones separate out across a concentration shock. Since there are no large particles on either side of  $OB$ , the large particle shock condition (8.13) is trivially satisfied. While the small particle jump condition (8.14) implies

$$\frac{d\psi}{dx} = S_{ms}\phi_1^s = w_1^m, \quad (8.19)$$



where the right-hand side is equal to the normal velocity of the medium-sized particles  $w_1^m$  in the bi-disperse region  $\mathcal{R}_1$ . This can be integrated subject to the condition that  $\psi(0) = 0$ , to show that the shock  $OB$  is also a straight line

$$\psi_{OB} = S_{ms}\phi_1^s x. \quad (8.20)$$

The two shocks  $OA$  and  $OB$ , shown in figure 10, that emanate from the base of the inflow have therefore been determined. This structure will be termed a double shock.

An exactly analogous procedure can be used to determine the double-shock structure at the top of the avalanche. The boundary conditions (2.33) imply that at the surface there is no further supply of medium and small particles. Assuming that the small particles percolate downwards fastest in the homogeneous mixture, the large and the medium particles will separate out across the shock  $1A$ . The small particle jump (8.14) gives an equation for the shock position

$$\frac{d\psi}{dx} = -S_{ls}\phi_0^l - S_{ms}\phi_0^m = w_0^s, \quad (8.21)$$

where the right-hand side is just the normal velocity  $w_0^s$  of the small particles in the homogeneous region. This can be integrated subject to the boundary condition that  $\psi(0) = 1$ , to show that the shock  $1A$  is the straight line

$$\psi_{1A} = 1 - (S_{ls}\phi_0^l + S_{ms}\phi_0^m)x. \quad (8.22)$$

Substituting the gradient (8.21) into the shock condition for the large particles

$$(\phi_2^l - \phi_0^l)\frac{d\psi}{dx} = S_{lm}(\phi_2^l\phi_2^m - \phi_0^l\phi_0^m) - S_{ls}\phi_0^l\phi_0^s, \quad (8.23)$$

and, using the fact that  $\phi_2^m = 1 - \phi_2^l$ , yields a quadratic equation

$$S_{lm}(\phi_2^l)^2 - (S_{ls}\phi_0^l + S_{ms}\phi_0^m + S_{lm})\phi_2^l + (S_{lm}\phi_0^m + S_{ls}(1 - \phi_0^m) + S_{ms}\phi_0^m)\phi_0^l = 0 \quad (8.24)$$

for the concentration of large particles,  $\phi_2^l$ . The concentration of medium-sized particles  $\phi_2^m = 1 - \phi_2^l$  since  $\phi_2^s = 0$ . In the bi-disperse region  $\mathcal{R}_2$ , the large particles rise upwards and the medium particles percolate downwards, except near the upper boundary, where there are no more medium particles and the large grains separate out across the concentration shock  $1C$ . This time the small particle jump condition (8.14) is trivially satisfied, while the large particle jump condition (8.13) implies that

$$\frac{d\psi}{dx} = -S_{lm}\phi_2^l = w_2^m, \quad (8.25)$$

where the right-hand side is just the normal velocity of the medium-sized particles  $w_2^m$  in the bi-disperse region  $\mathcal{R}_2$ . This can be integrated subject to the condition that  $\psi(0) = 1$ , to show that the shock  $1C$  is also a straight line,

$$\psi_{1C} = 1 - S_{lm}\phi_2^l x, \quad (8.26)$$

completing the double-shock structure near the surface.

### 8.3. Distance for the large and the small particles to separate

The shocks  $OA$  and  $1A$  merge at point  $A$  at a downstream distance

$$x_A = \frac{1}{S_{lm}\phi_0^m + S_{ls}(1 - \phi_0^m) + S_{ms}\phi_0^m}, \quad (8.27)$$

which is independent of  $\phi_0^l$  and  $\phi_0^s$ . The denominator in (8.27) is the difference between the large and small particle velocities,  $w_0^l = S_{lm}\phi_0^m + S_{ls}\phi_0^s$  and  $w_0^s = -S_{ls}\phi_0^l - S_{ms}\phi_0^m$ ,

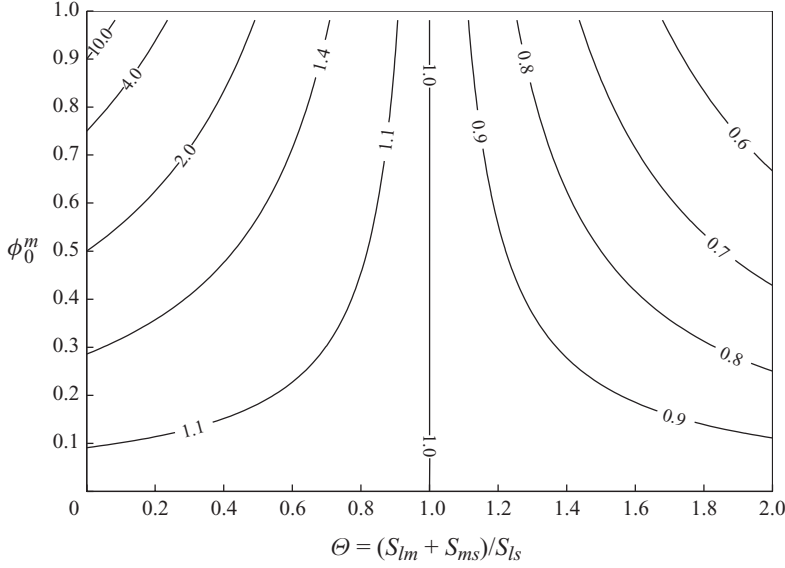


FIGURE 11. A contour plot of the ratio  $x_A/x_{ls}$ , between the distance for the large and small particles to segregate in a three-component mixture  $x_A$  and that in a two-component mixture  $x_{ls} = 1/S_{ls}$ , as a function of the inflow concentration of medium-sized particles  $\phi_0^m$  and the parameter  $\Theta = (S_{lm} + S_{ms})/S_{ls}$ . Note that  $x_A$  is not the distance for complete segregation in a three-component mixture, but does provide a lower bound.

in the homogeneous region. Point A therefore represents the distance over which a large particle rising up from the bottom meets a small particle percolating down from the top. The equivalent distance in a bi-disperse mixture is the point,  $x_{ls} = 1/S_{ls}$ , which is also the point of complete separation. In the three-component mixture, the segregation has not finished. However, it is still interesting to consider the ratio of these length scales as it provides a lower bound on the total segregation distance in the three-component case. By defining the parameter

$$\Theta = \frac{S_{lm} + S_{ms}}{S_{ls}}, \quad (8.28)$$

which typically lies in the range  $[0, 2]$  for the solution presented here, the ratio of the length scales can be written in the particularly simple form

$$\frac{x_A}{x_{ls}} = \frac{1}{1 + \phi_0^m (\Theta - 1)}. \quad (8.29)$$

This is plotted in figure 11 as a function of the inflow concentration of medium-sized particles  $\phi_0^m$  and the parameter  $\Theta$ . To understand the contour plot, it is useful to consider some special cases. If the inflow concentration  $\phi_0^m$  is equal to zero, the three-component problem has no medium-sized particles and it degenerates to the two-component case. The ratio is therefore equal to unity along the  $\Theta$ -axis. In the case where all the segregation rates are the same  $S_{ls} = S_{lm} = S_{ms}$ , the parameter  $\Theta = 2$ , and the large and small percolation velocities reduce to  $w_0^l = S_{ls}(1 - \phi_0^l)$  and  $w_0^s = -S_{ls}(1 - \phi_0^s)$ , respectively. It follows that as the volume fraction of medium-sized particles increases, the large and small particles can move at velocities closer to their maximum rates, since  $\phi_0^l$  and  $\phi_0^s$  are lower on average. The net velocity  $w_0^l - w_0^s = S_{ls}(1 + \phi_0^m)$  is therefore enhanced and the large and small particles separate

out from one another faster than the bi-disperse case. Note that this does not imply that the time for complete segregation is reduced. When  $\Theta = 0$ , which occurs when  $S_{lm} = S_{ms} = 0$ , the velocity of the large and small particles is  $w_0^l = S_{ls}\phi_0^s$  and  $w_0^s = -S_{ls}\phi_0^l$ . These look very similar to those for  $\Theta = 2$ , but this time, as the volume fraction of  $\phi_0^m$  increases, the large and the small particles move slower on average. Indeed the net velocity  $w_0^l - w_0^s = S_{ls}(1 - \phi_0^m)$  tends to zero as  $\phi_0^m \rightarrow 1$  and the segregation distance in the three-component mixture  $x_A \rightarrow \infty$ . In summary, if  $\Theta < 1$  the medium-sized particles hinder the separation of large and small grains. While if  $\Theta > 1$ , the medium particles allow the large and small grains to percolate faster than in the bi-disperse case, during this initial phase of segregation.

#### 8.4. Separation of the medium-sized particles

The height of point A can either be expressed using (8.16) as

$$\psi_A = (S_{lm}\phi_0^m + S_{ls}\phi_0^s)x_A, \quad (8.30)$$

or using (8.22) as

$$\psi_A = 1 - (S_{ls}\phi_0^l + S_{ms}\phi_0^m)x_A. \quad (8.31)$$

The equations for the position of point A, (8.27), (8.30) and (8.31), can be used to significantly simplify the quadratic equations (8.18) and (8.24) for the concentrations  $\phi_2^l$  and  $\phi_1^s$ , which become

$$S_{lm}x_A(\phi_2^l)^2 - (1 - \psi_A + S_{lm}x_A)\phi_2^l + \phi_0^l = 0, \quad (8.32)$$

$$S_{ms}x_A(\phi_1^s)^2 - (\psi_A + S_{ms}x_A)\phi_1^s + \phi_0^s = 0. \quad (8.33)$$

Point A is also the position at which two reflected shocks are generated, which are denoted by AB and AC in figure 10. The section AB separates the mixture of medium and small particles from a pure region of medium-sized particles. The large particle jump condition is therefore trivially satisfied. While the small particle jump condition implies that

$$\frac{d\psi}{dx} = -S_{ms}\phi_1^m = w_1^s, \quad (8.34)$$

where the right-hand side is simply the normal velocity  $w_1^s$  of the small particles in the bi-disperse region  $\mathcal{R}_1$ . Integrating subject to the condition that  $\psi(x_A) = \psi_A$  gives the straight line

$$\psi_{AB} = \psi_A - S_{ms}\phi_1^m(x - x_A). \quad (8.35)$$

The lines OB and AB intersect at a downstream distance

$$x_B = \frac{\psi_A}{S_{ms}} + \phi_1^m x_A. \quad (8.36)$$

The height at which this occurs can be determined by substituting (8.36) into the equation for the shock OB, given by (8.20), to obtain

$$\psi_B = (\psi_A + S_{ms}x_A)\phi_1^s - S_{ms}x_A(\phi_1^s)^2. \quad (8.37)$$

Using the quadratic equation (8.33), gives the simple result

$$\psi_B = \phi_0^s. \quad (8.38)$$

The small particle jump condition for the shock 'B $\infty$ ', separating the layer of medium-sized particles from the layer of fines below, implies that the gradient  $d\psi/dx$  is

zero. Integrating subject to the condition that  $\psi(x_B) = \psi_B$  implies that the shock is horizontal and is given by

$$\psi_{B\infty} = \psi_B, \quad x > x_B. \quad (8.39)$$

An analogous argument holds for the shock  $AC$  between the mixture of large and medium-sized particles in  $\mathcal{R}_2$  and the pure state of large particles at the surface. The large particle jump condition implies that

$$\frac{d\psi}{dx} = S_{lm}\phi_2^m = w_2^l, \quad (8.40)$$

where the right-hand side is just the normal velocity of the large particles in the bi-disperse region  $\mathcal{R}_2$ . This can be integrated subject to the condition that  $\psi(x_A) = \psi_A$ , to give the straight line

$$\psi_{AC} = \psi_A + S_{lm}\phi_2^m(x - x_A). \quad (8.41)$$

It intersects with  $1C$  at

$$x_C = \frac{1 - \psi_A}{S_{lm}} + \phi_2^m x_A. \quad (8.42)$$

The height of the intersection can be found by substituting (8.42) into (8.26) and using the quadratic equation (8.32) to show that

$$\psi_C = 1 - \phi_0^l. \quad (8.43)$$

At the inversely graded interface between the pure phases of large- and medium-sized particles, the large particle jump condition implies that  $d\psi/dx = 0$ . Integrating subject to the condition that  $\psi(x_C) = \psi_C$  implies that the final shock

$$\psi_{C\infty} = \psi_C, \quad x > x_C, \quad (8.44)$$

which completes the solution. The complete structure consists of six constant concentration regions that are separated by eight shocks given by (8.16), (8.20), (8.22), (8.26), (8.35), (8.39), (8.41) and (8.44).

### 8.5. Inverse mappings to physical coordinates

The advantage of using depth-integrated velocity coordinates (8.12) is that the solution is valid for all monotonically increasing velocity profiles with  $z$ . To view the solution for specific cases, the downstream velocity profile  $u(z)$  must be prescribed. Figure 12 shows four examples, one for an exponential velocity profile and three linear profiles. The linear profiles are all special cases of the linear downstream velocity of Gray & Thornton (2005), which was defined by the function

$$u = \alpha + 2(1 - \alpha)z, \quad 0 \leq \alpha \leq 1. \quad (8.45)$$

The parameter  $\alpha$  allows different amounts of shear and basal slip, while still ensuring that the depth-averaged velocity is unity. There are two special cases,  $\alpha = 0$  corresponds to simple shear and  $\alpha = 1$  implies plug flow. The mapped coordinates are calculated by performing the integral (8.12) to give

$$\psi = \alpha z + (1 - \alpha)z^2. \quad (8.46)$$

For plug flow, when  $\alpha = 1$ , the mapped and the physical coordinates are the same and the shocks are all straight lines as shown in figure 12(d). This situation can also be mapped from  $(x, z)$  to  $(t, z)$  to obtain time-dependent shock solutions, such as those indicated by the solid lines in figure 8. When there is shear, (8.46) is a quadratic

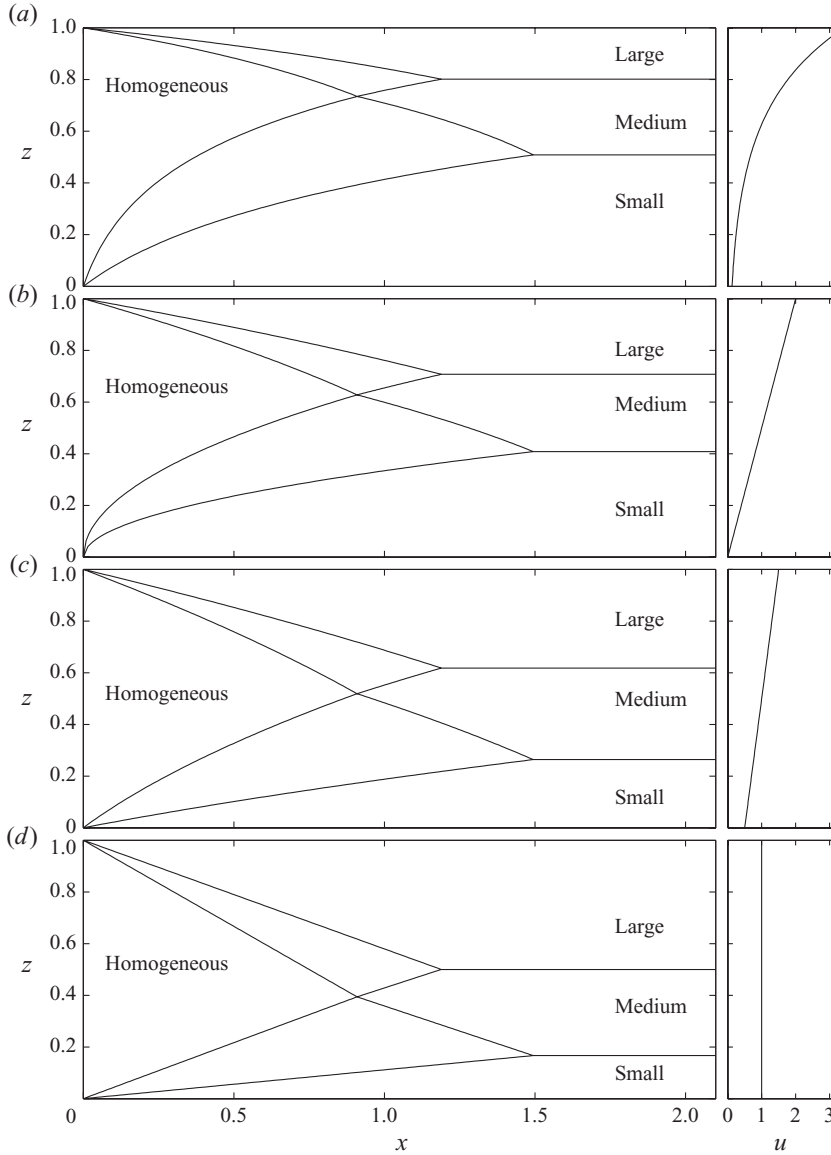


FIGURE 12. The left-hand panels show the shock heights as a function of  $(x, z)$  for segregation parameters  $S_{ls}=1$ ,  $S_{lm}=0.8$  and  $S_{ms}=0.5$ , inflow concentrations  $\phi_0^l=1/2$ ,  $\phi_0^s=1/6$  and  $\phi_0^m=1/3$ , and for the prescribed downstream velocity profiles  $u(z)$  shown in the corresponding right-hand panels. The graphs in (a) show an exponential velocity profile with  $\beta=3.3$ , (b) corresponds to simple shear,  $\alpha=0$ , (c) corresponds to shear with basal slip,  $\alpha=0.5$ , and (d) corresponds to plug flow,  $\alpha=1$ .

equation in  $z$  and the inverse mapping is

$$z = \frac{-\alpha + \sqrt{\alpha^2 + 4(1-\alpha)\psi}}{2(1-\alpha)}, \quad \alpha \neq 1. \quad (8.47)$$

This is equivalent to a nonlinear stretch of the  $\psi$  coordinate, so the shocks which were straight lines in the mapped coordinates now become curved in physical coordinates,

as shown in figure 12(b,c). The only lines that do not get stretched into curves are those that are parallel to the base, such as the final inversely graded shocks  $\psi_{B\infty}$  and  $\psi_{C\infty}$ , which get translated to new heights  $z_{B\infty}$  and  $z_{C\infty}$  in the physical domain. The reason for this is that there is a higher mass flux near the surface than at the base. At the inflow the particles enter at a homogenous concentration at all levels in the flow, and, because this is a steady problem, the depth-averaged flux of those particles is constant all along the chute. It follows that if the particles rise on average, the mass flux will be concentrated in a higher faster moving part of the flow, and hence the layer will be thinner than if they moved to lower slower moving regions. The large particle layer near the surface therefore becomes much thinner in the mapped domain, while the small particle layer near the base becomes much thicker.

Wiederseiner *et al.* (2011) found that the effect of the nonlinear velocity profile was quite strong in their chute flow experiments, and they needed to use an exponential fit to the velocity data that they measured in their experiments to get good agreement with the layer heights in their final steady uniform state. In order to compare their experiments with the theory of Gray & Chugunov (2006), they used a downstream velocity profile of the form

$$u = \frac{\beta \exp(\beta z)}{\exp(\beta) - 1}, \quad \beta > 0. \quad (8.48)$$

The depth-integrated velocity coordinates for this function are

$$\psi = \frac{\exp(\beta z) - 1}{\exp(\beta) - 1}, \quad (8.49)$$

and the corresponding inverse mapping is

$$z = \frac{1}{\beta} \ln(1 - \psi + \psi \exp(\beta)). \quad (8.50)$$

Figure 12(a) plots the shock solution for the exponential profile with Wiederseiner *et al.*'s (2011) measured coefficient of  $\beta = 3.3$ . The compression of the surface layer of large particles is very strong, taking a layer that occupied half the height in the mapped coordinates and squeezing it into the top fifth of the flow. Conversely, the small particle layer, which occupied a sixth of the height in the unmapped coordinates, is stretched out over half the flow height.

It should be noted that downstream positions of the shock intersection points are unchanged by the mapping, and so they lie at the same downstream distances in each of the three sets of plots in figure 12. Since  $\Theta = (S_{lm} + S_{ms})/S_{ls}$  is equal to 1.3, the graph in figure 11 shows that the point at which the large and the small particles separate out lies before the point  $x_{ls} = 1/S_{ls} = 1$ , where they would separate out in a bi-disperse mixture. However, the final distances for the complete segregation of the large- and medium-sized particles,  $x_C$ , and the medium and small grains  $x_B$ , occur significantly further down the chute than in the bi-disperse case. This is indicative of the general tendency of multi-component mixtures to extend the maximum distance for segregation.

#### 8.6. Parameter range of validity

The solution that has been constructed is not valid over the whole range of segregation parameters and inflow concentrations. The crucial condition for existence of the solution is that the topology of the shocks is preserved. This is true provided point A is higher than point B, but lower than point C, the gradient of the shock AB is

negative and the gradient of the shock  $AC$  is positive. Using (8.34) and (8.40) implies that these statements are equivalent to

$$\psi_B \leq \psi_A \leq \psi_C, \quad \phi_1^m \geq 0, \quad \phi_2^m \geq 0. \quad (8.51)$$

These conditions automatically ensure that the order of the discontinuities that have been assumed in the double-shock structures is preserved. Substituting the heights of points  $A$  and  $B$  from (8.30) and (8.38) into the condition  $\psi_B < \psi_A$  implies that

$$S_{lm} \geq \phi_0^s (S_{lm} - S_{ls} + S_{ms}). \quad (8.52)$$

By collecting the coefficients of  $S_{lm}$  together, substituting  $1 - \phi_0^s = \phi_0^m + \phi_0^l$  and using the definitions of the constituent velocities (8.5) and (8.6), it follows that this is equivalent to the normal velocity of the larger particles being greater than the normal velocity of medium-sized particles in the homogeneous mixture

$$w_0^l \geq w_0^m, \quad (8.53)$$

which was assumed in our derivation. If the factor  $S_{lm} - S_{ls} + S_{ms}$  in (8.52) is negative, then the right-hand side is at most equal to zero, and the condition is trivially satisfied as  $S_{lm}$  is positive. If  $S_{lm} - S_{ls} + S_{ms}$  is positive, then the right-hand side is largest when  $\phi_0^s$  equals unity, and (8.52) is satisfied, for all concentrations, provided

$$S_{ls} \geq S_{ms}. \quad (8.54)$$

Similarly, substituting (8.30) and (8.43) into the condition  $\psi_A < \psi_C$  implies that

$$S_{ms} \geq \phi_0^l (S_{lm} - S_{ls} + S_{ms}), \quad (8.55)$$

which, using (8.6) and (8.7), is equivalent to the condition that the small particles in the homogeneous mixture percolate downwards faster than the medium-sized particles,

$$w_0^s \geq w_0^m. \quad (8.56)$$

If the factor  $S_{lm} - S_{ls} + S_{ms}$  is negative, then condition (8.55) is trivially satisfied since  $S_{ms}$  is positive. If the factor  $S_{lm} - S_{ls} + S_{ms}$  is positive, then the right-hand side is largest when  $\phi_0^l$  is equal to unity, and the condition is satisfied, for all inflow concentrations, provided

$$S_{ls} \geq S_{lm}. \quad (8.57)$$

The condition that  $\phi_1^m \geq 0$  in the bi-disperse region  $\mathcal{R}_1$  is equivalent to the requirement that  $\phi_1^s \leq 1$ . The negative root of the quadratic equation (8.33) can be written in the form

$$\phi_1^s = \frac{\psi_A + S_{ms}x_A - \sqrt{(\psi_A - S_{ms}x_A)^2 + 4(\psi_A - \phi_0^s)S_{ms}x_A}}{2S_{ms}x_A}, \quad (8.58)$$

where the discriminant has been re-factored. Equation (8.38) implies that  $\phi_0^s = \psi_B$ , which is less than or equal to  $\psi_A$  by the first condition in (8.51). The smallest value reached by the square-root term in (8.58) is  $\psi_A - S_{ms}x_A$ , and hence the largest that  $\phi_1^s$  can be is unity. It is also clear from this equation that when  $\phi_0^s$  equals zero,  $\phi_1^s$  is also equal to zero, and hence that  $\phi_1^s \in [0, 1]$ . It follows that  $\phi_1^m \in [0, 1]$  and the third condition in (8.51) is satisfied. Similarly, the condition  $\phi_2^m \geq 0$  in the bi-disperse region  $\mathcal{R}_2$  is equivalent to the condition  $\phi_2^l \leq 1$ . The negative root of the quadratic equation (8.32) implies that the concentration of large particles is

$$\phi_2^l = \frac{1 - \psi_A + S_{lm}x_A - \sqrt{(1 - \psi_A - S_{lm}x_A)^2 + 4(1 - \phi_0^l - \psi_A)S_{lm}x_A}}{2S_{lm}x_A}, \quad (8.59)$$

where the discriminant has again been re-factored. Equation (8.43) implies that  $1 - \phi_0^l = \psi_C$ , which is greater than or equal to  $\psi_A$  by the second condition in (8.51). The smallest value reached by the square-root term in (8.59) is,  $1 - \psi_A - S_{lm}x_A$ , and hence the largest concentration can be unity. It is also clear that when  $\phi_0^l$  is equal to zero, the large particle concentration is equal to zero, and hence  $\phi_2^l \in [0, 1]$ . It follows that  $\phi_2^m \in [0, 1]$  and hence the final condition in (8.51) is satisfied.

All conditions for existence are therefore satisfied provided the normal velocities of the constituents in the homogeneous region are such that  $w_0^l \geq w_0^m \geq w_0^s$ , and this can be guaranteed, for all concentrations, provided the segregation parameters lie in the domain

$$\Omega_3^+: \quad S_{ls} \geq S_{lm} \quad \text{and} \quad S_{ls} \geq S_{ms}. \quad (8.60)$$

Note that this is slightly larger than the region  $\Omega_3$ , defined in (5.20). The time-dependent shock solution illustrated by solid lines in figure 8 is obtained by setting  $\alpha = 1$  and replacing  $x$  by  $t$ , and  $\psi$  by  $z$ , in the two-dimensional steady-state solution derived here. It closely approximates the perturbed numerical solution when  $D_r$  is small and provides an example of this solution in a region outside of  $\Omega_3^+$  that holds for certain values of the initial conditions. It cannot, of course, capture the linear sawtooth instability in figure 9, which develops for the same parameters, but slightly different initial conditions.

### 8.7. Upper and lower bounds for the total segregation distance

It would be useful to have a simple estimate for the total segregation length that could easily be computed from the initial conditions. Let us therefore return to the quadratic equation (8.18), substitute for the concentration of medium-sized particles and write it in the form

$$\begin{aligned} S_{ms}((\phi_1^s)^2 - (\phi_0^s)^2) - (S_{lm}(1 - \phi_0^s) + S_{ls}\phi_0^s + S_{ms})(\phi_1^s - \phi_0^s) \\ + \phi_0^l(S_{lm}(\phi_1^s - \phi_0^s) + \phi_0^s(S_{ls} - S_{ms})) = 0, \end{aligned} \quad (8.61)$$

where all the terms involving  $\phi_0^l$  are gathered together. If the large particle inflow concentration  $\phi_0^l$  is equal to zero, it is then easy to see that the concentration of small particles  $\phi_1^s$  in region  $\mathcal{R}_1$  is equal to the inflow concentration

$$\phi_1^s = \phi_0^s. \quad (8.62)$$

Figure 13 shows a contour plot of the negative root of the quadratic equation (8.58) as a function of the inflow concentrations  $\phi_0^l$  and  $\phi_0^s$  for a specific case of segregation parameters that lie in  $\Omega_3^+$ . Along the  $\phi_1^l$ -axis the solution is zero, along the  $\phi_0^s$ -axis the concentration is equal to the inflow concentration, and above the line  $\phi_0^l = 1 - \phi_0^s$  the concentration states are not admissible. The plot shows that for a fixed value of  $\phi_0^s$ , the bi-disperse concentration is greater than or equal to the inflow concentration

$$\phi_1^s \geq \phi_0^s. \quad (8.63)$$

This suggests that it is possible to be more specific about the range of values of  $\phi_1^s$  in  $\mathcal{R}_1$  than in §8.6 and hence provide a useful estimate of the total segregation distance of the small particles.

We have already shown in (8.62) that, when there are no large particles, the bi-disperse concentration  $\phi_1^s$  is equal to the inflow concentration  $\phi_0^s$  for all values of the segregation parameters. Let us now consider what happens as the concentration of large particles is increased. Taking the partial derivative of the quadratic equation



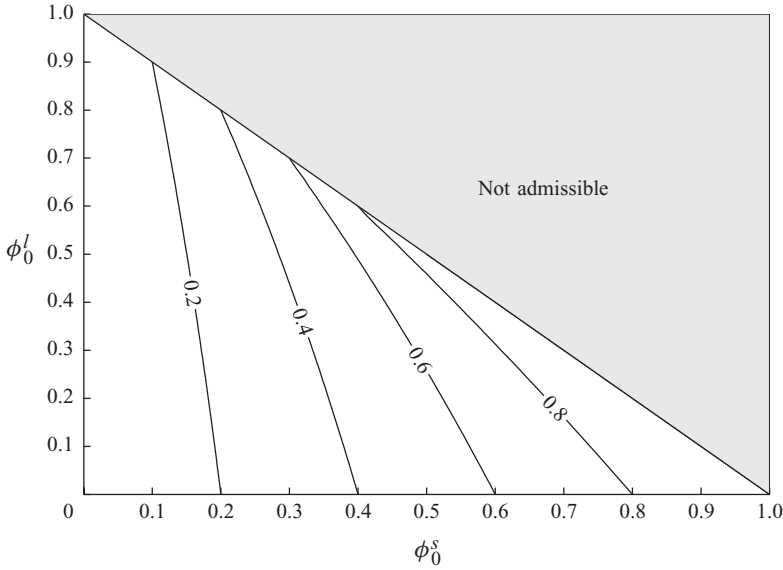


FIGURE 13. A contour plot of the small particle concentration,  $\phi_1^s$ , in the bi-disperse region  $\mathcal{R}_1$  as a function of the inflow concentrations  $\phi_0^l$  and  $\phi_0^s$  and for segregation parameters  $S_{ls} = 1$ ,  $S_{lm} = 0.8$  and  $S_{ms} = 0.5$ . Note that the region above the line  $\phi_0^l = 1 - \phi_0^s$  corresponds to concentration states that are not possible.

(8.61) with respect to the large particle inflow concentration  $\phi_0^l$  implies that

$$\frac{\partial \phi_1^s}{\partial \phi_0^l} = \frac{S_{lm}(\phi_1^s - \phi_0^s) + \phi_0^s(S_{ls} - S_{ms})}{S_{ms}(1 - \phi_1^s) + [S_{lm}\phi_0^m + S_{ls}\phi_0^s - S_{ms}\phi_1^s]}. \quad (8.64)$$

Whether  $\phi_1^s$  increases or decreases from the inflow value  $\phi_0^s$  at  $\phi_0^l = 0$  is dependent on whether this derivative is positive or negative. The square-bracketed term in the denominator is the difference in the gradients of the shocks  $0A$  and  $0B$  by (8.15) and (8.19). Provided the solution exists, i.e. the conditions (8.51) are satisfied and the order of the double shock structure is preserved, the square-bracketed term is positive. It follows that the denominator is strictly positive, since  $\phi_1^s \in [0, 1]$ , except in the completely degenerate case of pure fines. The behaviour is therefore controlled by the sign of the numerator in (8.64). If  $S_{ls} > S_{ms}$ , then on the line  $\phi_0^l = 0$ , where  $\phi_1^s = \phi_0^s$ , the numerator is strictly positive and hence  $\phi_1^s$  will increase in the direction of increasing  $\phi_0^l$ , again provided that the system is not in the completely degenerate case of pure fines. The solution may therefore be continued to an adjacent strip where  $\phi_1^s > \phi_0^s$ . Since the numerator is still positive here, and on every other adjacent strip, the small particle concentration  $\phi_1^s \in [\phi_0^s, 1]$ . A similar argument for the case  $S_{ls} = S_{ms}$  shows that  $\phi_1^s$  is equal to  $\phi_0^s$ , for all values of  $\phi_0^l$ , since the numerator is always zero, while for  $S_{ls} < S_{ms}$  the numerator is always negative and therefore  $\phi_1^s \in [0, \phi_0^s]$ .

Let us restrict ourselves to the case where  $S_{ls} \geq S_{ms}$  and  $\phi_1^s \in [\phi_0^s, 1]$ . Consider what happens to the shock  $0B$  when  $\phi_1^s$  is replaced with its lower bound  $\phi_0^s$  in (8.20), to give the line

$$\psi = S_{ms}\phi_0^s x. \quad (8.65)$$

This represents the minimum height of the shock and is shown by the lower dot-dashed line in figure 14. It intersects with the shock  $B\infty$ , which lies at a height  $\psi_B = \phi_0^s$

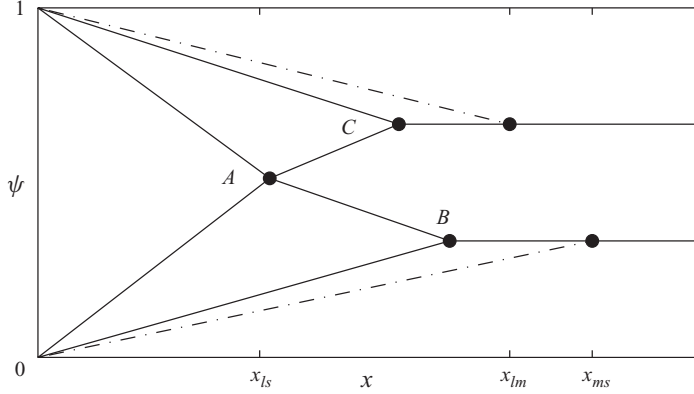


FIGURE 14. A sketch of the shocks (solid lines) in  $(x, \psi)$ -mapped coordinates with the key shock intersection points  $A$ ,  $B$  and  $C$ . The dot-dashed lines represent lower bounds for the modulus of the shock gradients that emanate from  $(0, 0)$  and  $(0, 1)$ , and they therefore intersect with horizontal inversely graded shocks, ' $B\infty$ ' and ' $C\infty$ ', furthest downstream at  $x_{ms}$  and  $x_{lm}$ , respectively. The distance  $x_{ls}$  is the segregation distance of the large and small particles, which may be before or after the downstream position of point  $A$ .

at a downstream distance

$$x_{ms} = \frac{1}{S_{ms}}. \quad (8.66)$$

This is just the distance over which a bi-disperse mixture of medium and small particles would segregate out, and it forms an upper bound for the segregation of the medium and the small particles in a ternary mixture when  $S_{ls} \geq S_{ms}$ . Note that when  $S_{ls} < S_{ms}$ , then (8.66) represents a lower bound instead.

A very similar argument gives an upper bound at the surface. Rewriting the quadratic equation (8.24) in the form

$$S_{lm}((\phi_2^l)^2 - (\phi_0^l)^2) - (S_{ms}(1 - \phi_0^l) + S_{ls}\phi_0^l + S_{lm})(\phi_2^l - \phi_0^l) + \phi_0^s(S_{ms}(\phi_s^l - \phi_0^l) + \phi_0^l(S_{ls} - S_{lm})) = 0, \quad (8.67)$$

it is easy to see that it has the solution

$$\phi_2^l = \phi_0^l, \quad (8.68)$$

when the inflow concentration  $\phi_0^s$  is zero. Taking the partial derivative of the quadratic equation (8.67) with respect to  $\phi_0^s$  implies that

$$\frac{\partial \phi_2^l}{\partial \phi_0^s} = \frac{S_{ms}(\phi_2^l - \phi_0^l) + \phi_0^l(S_{ls} - S_{lm})}{S_{lm}(1 - \phi_2^l) + [S_{ls}\phi_0^l + S_{ms}\phi_0^m - S_{lm}\phi_2^l]}. \quad (8.69)$$

The square-bracketed term is the difference between the gradients of 1A and 1C and is positive provided that existence conditions (8.51) are satisfied. Since  $\phi_2^l \in [0, 1]$ , it follows that the denominator is strictly positive, except in the completely degenerate case of all large particles. If  $S_{ls} > S_{lm}$  then the numerator is strictly positive on the line  $\phi_0^s = 0$ , since  $\phi_2^l = \phi_0^l$ . The solution may therefore be continued to an adjacent strip where  $\phi_2^l > \phi_0^l$ . Since the numerator is still positive here, and on every other adjacent strip,  $\phi_2^l \in [\phi_0^l, 1]$ . Similar arguments show that if  $S_{ls} = S_{lm}$  then  $\phi_2^l = \phi_0^l$ , and if  $S_{ls} < S_{lm}$  then the large particle concentration  $\phi_2^l \in [0, \phi_0^l]$ . Restricting ourselves to the case  $S_{ls} \geq S_{lm}$ , and using the lower bound  $\phi_0^l$  to replace  $\phi_2^l$  in (8.26) for the shock

OC, gives the line

$$\psi = 1 - S_{lm}\phi_0^l x. \quad (8.70)$$

This represents the maximum height that the shock can reach and is shown by the upper dot-dashed line in figure 14. It intersects with the shock ‘C $\infty$ ’, which lies at a height  $\psi_C = 1 - \phi_0^l$  at a downstream distance

$$x_{lm} = \frac{1}{S_{lm}}, \quad (8.71)$$

which is just the distance that a bi-disperse mixture of large- and medium-sized particles would separate out. It forms an upper bound for the segregation of the large and the medium grains in a ternary mixture when  $S_{ls} \geq S_{lm}$ . When  $S_{ls} < S_{lm}$  then (8.71) represents a lower bound. It may therefore be concluded that an upper bound for the total segregation distance from a homogeneous inflow in a ternary mixture, with segregation parameters that lie in  $\Omega_3^+$ , is

$$x_{total} \leq \max(x_{lm}, x_{ms}) = \max\left(\frac{1}{S_{lm}}, \frac{1}{S_{ms}}\right). \quad (8.72)$$

Physically, this is simply the idea that, in a ternary mixture where the large and the small grains segregate fastest, an upper bound for the maximum segregation distance is given by the segregation length scale of the bi-disperse sub-mixture that segregates least well. Note that in the case where  $S_{ls} = S_{lm} = S_{ms}$ , the upper bound is equal to the total segregation length scale,  $x_{ls} = 1/S_{ls}$ , which is precisely the same as the bi-disperse case. The situation for mixtures with segregation parameters outside  $\Omega_3^+$  is more complex. This is firstly because it cannot be guaranteed that a solution with the proposed shock structure exists, or that the problem is even well-posed, as shown in § 5. Moreover, the estimates, (8.66) and (8.71), may be lower bounds.

## 9. Steady solutions of the segregation–remixing equations

Segregation theory yields considerable insight into the physical system, but to get good agreement with experiments it is important to include the diffusive terms. These account for the fluctuations in the avalanche that induce individual particles to take random walks, which smooth out the sharp concentration discontinuities that would otherwise form. It is therefore of interest to solve the same steady homogeneous inflow problem, but with the inclusion of the diffusive terms. Using the steady uniform bulk flow field (8.1), the segregation–remixing equations for the large and small particles (3.3)–(3.4) can be written in the flux conservative form

$$u \frac{\partial \phi^l}{\partial x} = \frac{\partial}{\partial z} \left( -S_{lm}\phi^l(1 - \phi^l - \phi^s) - S_{ls}\phi^l\phi^s + D_r \frac{\partial \phi^l}{\partial z} \right), \quad (9.1)$$

$$u \frac{\partial \phi^s}{\partial x} = \frac{\partial}{\partial z} \left( S_{ls}\phi^s\phi^l + S_{ms}\phi^s(1 - \phi^l - \phi^s) + D_r \frac{\partial \phi^s}{\partial z} \right). \quad (9.2)$$

These are precisely of the form required by standard Galerkin finite element solvers for initial boundary-value problems for systems of parabolic equations (e.g. Skeel & Berzins 1990). It is therefore very easy to solve practical multi-component segregation problems using standard programme libraries. In this paper, the pdepe routine contained in Matlab has been used. The initial conditions are given by (8.8) and the boundary conditions at the surface and the base of the avalanche need to be

formulated in terms of the fluxes of large and small particles, which are

$$\mathcal{F}^l = -S_{lm}\phi^l(1 - \phi^l - \phi^s) - S_{ls}\phi^l\phi^s + D_r \frac{\partial \phi^l}{\partial z}, \quad (9.3)$$

$$\mathcal{F}^s = S_{ls}\phi^s\phi^l + S_{ms}\phi^s(1 - \phi^l - \phi^s) + D_r \frac{\partial \phi^s}{\partial z}, \quad (9.4)$$

respectively. It is easy to see from this that the boundary conditions (2.32) reduce to

$$\mathcal{F}^v = 0, \quad z = 0, 1, \quad v = l, s. \quad (9.5)$$

This system can be integrated forward in  $x$  from the inflow at  $x=0$  to any distance downstream, to compute the steady-state concentrations of large and small particles  $\phi^l(x, z)$  and  $\phi^s(x, z)$ . The concentration of medium-sized particles can then be calculated from the summation condition (8.2). An example Matlab m-file using the exponential velocity profile (8.48) can be found in the supplementary material. The steady-state simulations in this paper were performed on a 200 node grid in  $z$ , using a relative error tolerance of  $10^{-6}$ . Although these Galerkin solvers are very robust, they cannot cope with very small non-dimensional diffusion coefficients or the zero diffusion limit.

In the scalings (2.24), the horizontal length scale  $L$  was left as general as possible to allow the theory to be easily incorporated into existing models for the bulk flow of granular materials on rough and smooth beds. In the simulations presented here, the bulk velocity field is prescribed. Without loss of generality,  $L$  is therefore chosen so that one of the segregation parameters  $S_{v\mu}$  is equal to unity. Figure 15 shows the results of a simulation of reverse distribution grading using segregation parameters  $S_{ls}=1$ ,  $S_{lm}=0.8$  and  $S_{ms}=0.5$ , and a relatively small diffusive remixing coefficient  $D_r=0.01$ . This is an example of a ternary mixture that lies in region  $\Omega_3^+$ , defined in (8.60), and the diffusive solution is expected to be close to the non-diffusive shock solution constructed in §8. The grey-shaded contour plots in figure 15(a–c) show the concentration of large, medium and small particles respectively. This way of representing the concentration is motivated by the time-averaged images that Wiederseiner *et al.* (2011) used to visualize the concentration in bi-disperse experiments. To obtain similar images for a ternary mixture, the experiments would have to be repeated three times, using dark particles for the constituent of interest, and light particles for the other two. For comparison with the non-diffuse case the shocks, which are not degenerate in that particle type, have been superposed on top of each concentration plot using solid lines. With a diffusion coefficient  $D_r=0.01$ , they very closely delineate the regions of high and low concentrations in the diffuse theory.

Figure 15(d) shows the concentration profile with depth of the large, medium and small particles at  $x=2.1$ , where the solution is close to its steady uniform state. Even though the large particle inflow concentration  $\phi_0^l=1/2$ , the large particles are compressed into a very thin near surface layer, due to the highly nonlinear exponential velocity field when  $\beta=3.3$ , as discussed in §8.5. In contrast, the small particles, which have an inflow concentration  $\phi_0^s=1/6$ , occupy nearly half the flow depth. The medium-sized particles, which are sandwiched in between, have an inflow concentration  $\phi_0^m=1/3$ . The layer is slightly thinner than an avalanche without any shear, but it lies considerably higher in the flow. The inverse length scale of the smooth transition between the inversely graded layers in the steady uniform state is set by the Péclet number,  $Pe$ . This is a measure of the ratio of the segregation transport rate to the rate of diffusion (Gray & Chugunov 2006). In a bi-disperse mixture, there is just

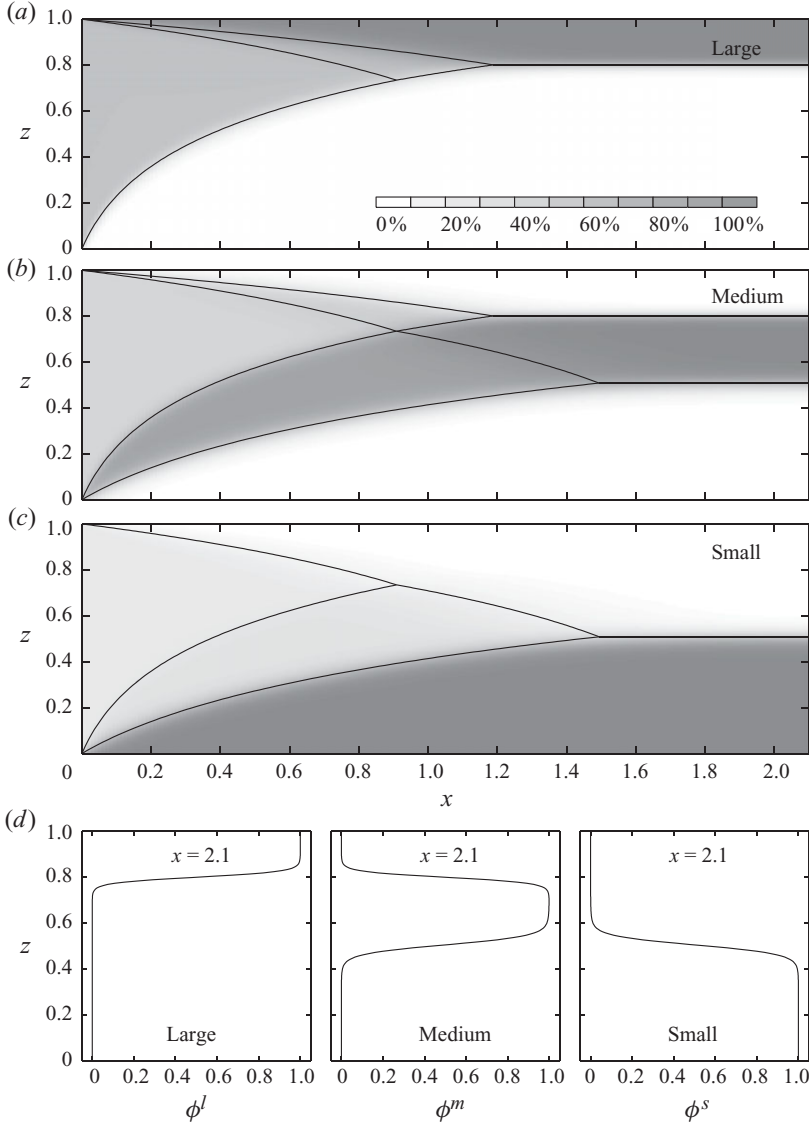


FIGURE 15. In (a–c) are shaded contour plots in  $(x, z)$  of the steady-state concentration of large, medium and small particles, for segregation parameters  $S_{ls} = 1$ ,  $S_{lm} = 0.8$  and  $S_{ms} = 0.5$ , inflow concentrations  $\phi_0^l = 1/2$ ,  $\phi_0^m = 1/3$  and  $\phi_0^s = 1/6$ , and an exponential velocity profile  $u(z)$  with  $\beta = 3.3$ . The diffusive remixing coefficient  $D_r = 0.01$ . For comparison with the non-diffusive case, the non-degenerate shocks are shown by solid lines. The plots use 64 grey levels and a scale with 11 levels is shown in (a). In (d), the final concentration profile at  $x = 2.1$  is plotted for the large, medium and small particles.

a single Péclet number, but in a ternary mixture there are three

$$Pe_{ls} = S_{ls}/D_r, \quad Pe_{lm} = S_{lm}/D_r, \quad Pe_{ms} = S_{ms}/D_r. \quad (9.6)$$

For the example in figure 15, these Péclet numbers are 100, 80 and 50, respectively. The length scale of the diffuse transition between medium and small particles is therefore slightly longer than that between medium and large particles in the steady

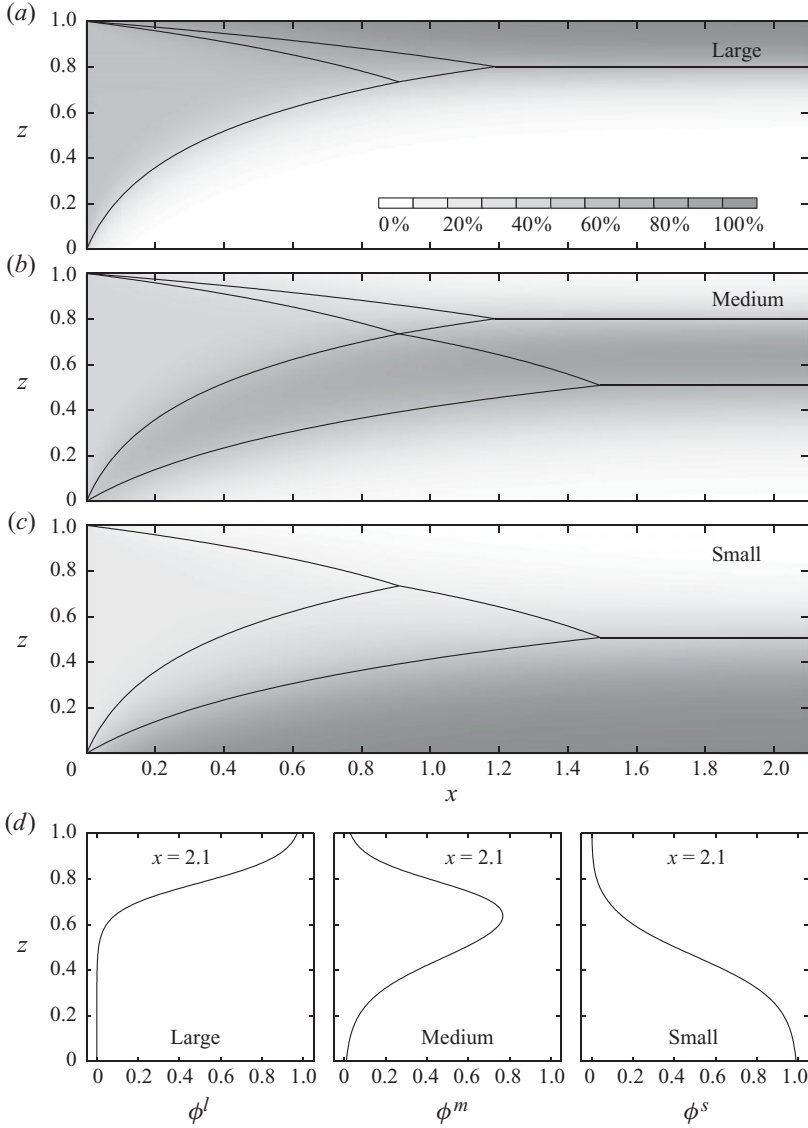


FIGURE 16. In (a–c) are shaded contour plots in  $(x, z)$  of the steady-state concentration of large, medium and small particles, for segregation parameters  $S_{ls} = 1$ ,  $S_{lm} = 0.8$  and  $S_{ms} = 0.5$ , inflow concentrations  $\phi_0^l = 1/2$ ,  $\phi_0^m = 1/3$  and  $\phi_0^s = 1/6$ , and an exponential velocity profile  $u(z)$  with  $\beta = 3.3$ . The diffusive remixing coefficient  $D_r = 0.05$ . For comparison with the non-diffusive case, the non-degenerate shocks are shown by solid lines. The plots use 64 grey levels and a scale with 11 levels is shown in (a). In (d), the final concentration profile at  $x = 2.1$  is plotted for the large, medium and small particles.

uniform state, although they are both sharp. Wiederseiner *et al.* (2011) inferred Péclet numbers between 10 and 20 from their bi-disperse experiments, and figure 16 shows another simulation with the same segregation parameters, inflow concentrations and exponential velocity field, but a diffusion coefficient  $D_r = 0.05$ . This gives Péclet numbers  $Pe_{ls} = 20$ ,  $Pe_{lm} = 16$  and  $Pe_{ms} = 10$ , which make these results potentially representative of real experiments. Indeed, the regions of high concentration of the

large, medium and small particles are very similar to the inversely graded avalanche at the surface of the rotating drum experiment shown in figure 2. The shock solutions, shown by lines in figure 16(a–c), still give an approximate position for regions of high concentrations of large medium and small particles, but the transitions are now much smoother. Indeed for a mixture with segregation parameters in  $\Omega_3^+$ , the transitions between the large and medium, and medium and small particles, are more smeared out than they would be for a bi-disperse mixture of large and small particles, because the Péclet numbers are lower. In general, as more constituents with lower relative segregation rates are added to the mixture, the steady uniform state will become increasingly diffuse and harder to measure and interpret. Nevertheless, even such diffuse segregation can have important consequences for the properties of the mixture and may have a feedback on the bulk motion of the grains.

## 10. Reverse coarse-tail grading

Geologists often encounter reverse coarse-tail grading in pyroclastic flow deposits (see e.g. Cas & Wright 1987; Branney & Kokelaar 1992; Palladino & Valentine 1995; Hiscott 2003). Although there is still some debate about exactly why it develops (Cagnoli & Manga 2005) and whether it is representative of the size distribution in the parent flow (Branney & Kokelaar 1992), it is possible to use the multi-component theory to produce a highly simplified model of it. Within the three-component mixture framework the coarse tail will comprise the large and the medium-sized particles and all the fine-grained material, which does not segregate from each other, will be lumped into a single class of small grains. Consider what happens when the small particles do not segregate from the large or the medium-sized particles either and the segregation rates are

$$S_{ls} = 0 \quad \text{and} \quad S_{ms} = 0. \quad (10.1)$$

This is a rather extreme example of a mixture that lies in the region of parameter space  $\Omega_2$ , defined in (5.11). With these assumptions, the steady-state segregation–remixing equations (9.1) and (9.2) reduce to

$$u \frac{\partial \phi^l}{\partial x} = \frac{\partial}{\partial z} \left( -S_{lm} \phi^l (1 - \phi^l - \phi^s) + D_r \frac{\partial \phi^l}{\partial z} \right), \quad (10.2)$$

$$u \frac{\partial \phi^s}{\partial x} = \frac{\partial}{\partial z} \left( D_r \frac{\partial \phi^s}{\partial z} \right), \quad (10.3)$$

where the last equation uncouples from the system. This is a simple diffusion equation and the initial concentration of small particles  $\phi^s(0, z)$  will therefore be diffused until it reaches a constant value throughout the avalanche depth. In the case of the homogeneous inflow problem, the initial condition (8.8) implies that it is already at a constant state  $\phi^s(0, z) = \phi_0^s$ . This will remain unchanged with increasing downstream distance. The same Galerkin finite element method, as described in §9, can be used to solve the system. The results are shown in figure 17 for the case  $S_{lm} = 1$  and  $D_r = 0.01$ . Figure 17(c) shows that the small particles are at the inflow concentration  $\phi_0^s$  throughout the avalanche as expected, while plots in figure 17(a,b) look very similar to the segregation structure in a bi-disperse mixture. There are, however, some subtle differences here. Firstly, the maximum concentrations of the large- and medium-sized particles is lower, because the small particles already take up one third of the available space, and secondly the distance for segregation is enhanced by the presence of the non-segregating small material.

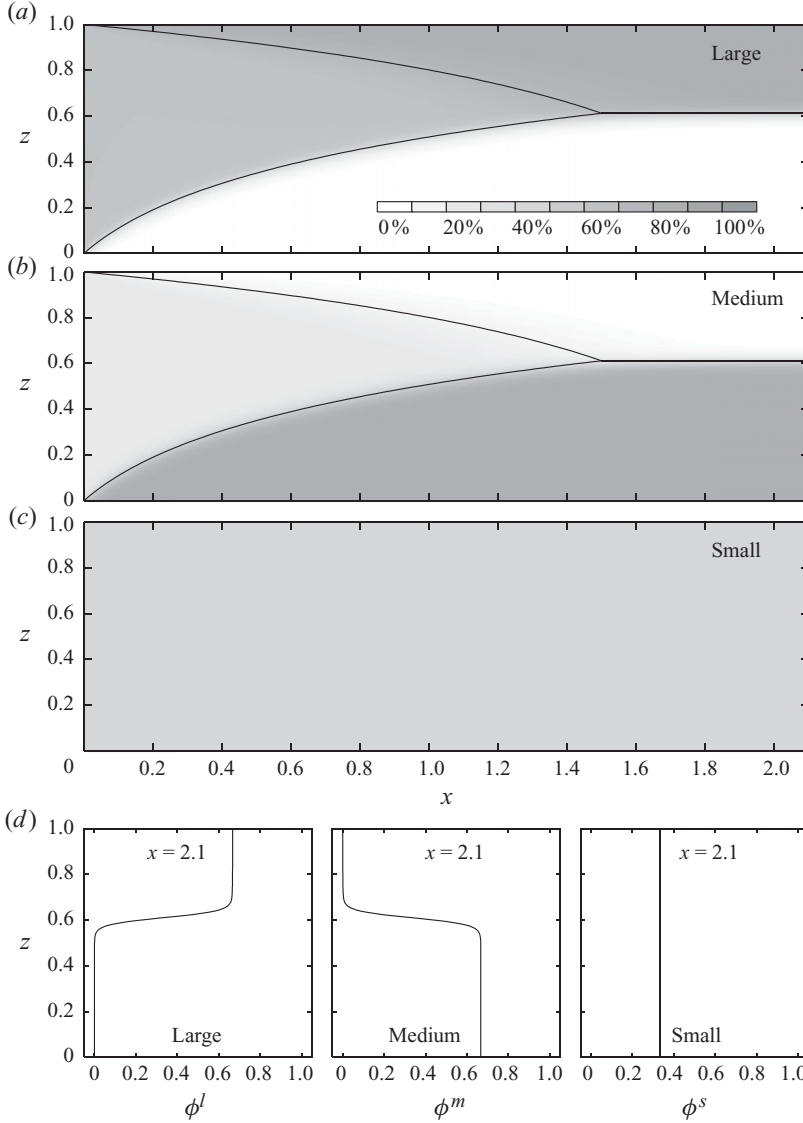


FIGURE 17. In (a–c) are shaded contour plots in  $(x, z)$  of the steady-state concentration of large, medium and small particles, for segregation parameters  $S_{ls} = 0$ ,  $S_{lm} = 1$  and  $S_{ms} = 0$ , inflow concentrations  $\phi_0^l = 1/2$ ,  $\phi_0^m = 1/6$  and  $\phi_0^s = 1/3$ , and an exponential velocity profile  $u(z)$  with  $\beta = 3.3$ . The diffusive remixing coefficient  $D_r = 0.01$ . For comparison with the non-diffusive case, the non-degenerate shocks are shown by solid lines. The plots use 64 grey levels and a scale with 11 levels is shown in (a). In (d), the final concentration profile at  $x = 2.1$  is plotted for the large, medium and small particles.

To understand this in greater detail, it is useful to consider the non-diffusive shock solution, which is shown using lines superposed on top of the contour plot in figure 17. In the absence of diffusion, (10.3) implies that the concentration of small particles is simply a function of height

$$\phi^s(x, z) = \phi^s(z), \quad (10.4)$$



which is set by the inflow conditions. In general, this is not equal to the diffusive solution, where the variations in the inflow concentration are smeared out and equilibrated with increasing downstream distance. However, for the special case of a homogeneous inflow, the condition (8.8) ensures that the small particle concentration is equal to the inflow concentration everywhere,

$$\phi^s(x, z) = \phi_0^s, \quad (10.5)$$

and the diffusive and non-diffusive cases are the same. The depth-averaged velocity coordinates  $(x, \psi)$  introduced in § 8 are again helpful in calculating the shock solution. The shocks are governed by the jump conditions (8.13)–(8.14). Since the small particle concentration does not jump across any of the shocks, (8.14) is trivially satisfied. However, the jump condition for the large particles (8.13) reduces to

$$[\![\phi^l]\!] \frac{d\psi}{dx} = [\![S_{lm}\phi^l(1 - \phi^l - \phi_0^s)]\!], \quad (10.6)$$

which implies that

$$\frac{d\psi}{dx} = S_{lm}(1 - \phi_0^s - \phi_+^l - \phi_-^l). \quad (10.7)$$

A shock develops at the base of the inflow between a region above where the large particle concentration is equal to the inflow concentration  $\phi_+^l = \phi_0^l$  and a region below where there are no large particles  $\phi_-^l = 0$ . The shock condition (10.7) can therefore be integrated subject to the condition that  $\psi(0) = 0$ , to show that the shock is

$$\psi = S_{lm}\phi_0^m x. \quad (10.8)$$

This is the same shock that would be expected for a bi-disperse mixture of large- and medium-sized particles (Gray & Thornton 2005). The shock that develops at the surface of the inflow is more subtle. In particular, it is important to reconsider the boundary condition (2.32) in the case of a non-segregating component and zero diffusion. For the small particles, the boundary condition (2.32) is trivially satisfied, for arbitrary concentrations of small particles, since the small particle segregation rates  $S_{vs}$  are zero for all  $v$  by (10.1). There is therefore no flux of small particles across the boundary. The boundary condition for the large particles then becomes

$$S_{lm}\phi^l\phi^m = 0, \quad (10.9)$$

which can be satisfied if either  $\phi^l$  or  $\phi^m$  equals zero. The first of these conditions was used at the base. However, the latter now implies that the large particle concentration on the forward side of the shock is

$$\phi_+^l = 1 - \phi_0^s, \quad (10.10)$$

as the small particle concentration is non-zero at the surface. The jump condition (10.7) with  $\phi_-^l = \phi_0^l$  can then be integrated subject to the condition that  $\psi(0) = 1$ , to show that the top shock is

$$\psi = 1 - S_{lm}\phi_0^l x, \quad (10.11)$$

which is not the same as the equivalent shock in a bi-disperse mixture of large- and medium-sized particles (Gray & Thornton 2005). The two shocks (10.8) and (10.11) intersect at a downstream distance

$$x_{\text{intersect}} = \frac{1}{S_{lm}(1 - \phi_0^s)}, \quad (10.12)$$

and at height

$$\psi_{\text{intersect}} = \frac{\phi_0^m}{1 - \phi_0^s}, \quad (10.13)$$

which are only the same as those for a bi-disperse mixture of large- and medium-sized particles (Gray & Thornton 2005) when there are no small particles,  $\phi_0^s = 0$ . The shock condition (10.7) implies that the final discontinuity, between states  $\phi_+^l = 1 - \phi_0^s$  above and  $\phi_-^l = 0$  below, is the slope parallel straight line

$$\psi = \psi_{\text{intersect}}, \quad x > x_{\text{intersect}}. \quad (10.14)$$

Using the inverse mapping (8.50) for the exponential downstream velocity field (8.48), the shocks can be mapped back to physical coordinates to give the lines shown in figure 17. Equation (10.12) shows that the introduction of the non-segregating small particle constituent significantly delays the segregation of the large and the medium particles. It raises it from its usual value of unity, when  $S_{lm} = 1$ , to 1.5 non-dimensional units for a concentration  $\phi_0^s = 1/3$ . This is also evident from the relative percolation velocity of the large- and medium-sized particles, which is given by the difference of (8.5) and (8.6),

$$w^l - w^m = S_{lm}(1 - \phi_0^s). \quad (10.15)$$

When  $\phi_0^s = 0$  the relative percolation velocity is the same as in the bi-disperse case, but as  $\phi_0^s$  is increased the relative percolation velocity in (10.15) decreases, and the distance for complete segregation (10.12) is increased. Physically, this is an expression of the fact that large particles will find it increasingly difficult to percolate downwards, if there are fewer gaps opening up between the medium-sized grains, because of the presence of the non-segregating fine-grained material. The presence of the small particles also necessarily reduces the maximum concentrations of the large and the medium particles, which can be seen in both the contour plots in figure 17(a,b) and the concentration profiles of the large and medium particles in figure 17(d).

If  $S_{ls} \ll S_{lm}$  and  $S_{ms} \ll S_{lm}$ , instead of being equal to zero, the segregation–remixing equations still yield solutions that look very similar to those in figure 17. The only difference is that the slow percolation of the fine grains is balanced by the diffusive remixing, which generates a shallow gradient of fines from top to bottom. This necessarily sets up corresponding gradients of medium and large grains that are only perceptible in the regions that would otherwise be at a constant concentration. However, when there is no diffusion, there is nothing to prevent the fines from segregating out and they eventually collect at the base of the flow. The segregation–remixing equations are therefore able to capture reverse coarse-tail grading for a poorly segregating phase, but the non-diffusive theory can only capture it for the rather extreme case considered here.

## 11. Discussion and conclusions

This paper significantly generalizes existing bi-disperse size-segregation/remixing theories for granular avalanches (Savage & Lun 1988; Dolgunin & Ukolov 1995; Gray & Thornton 2005; Gray & Chugunov 2006; Thornton *et al.* 2006) to the case of size segregation of an arbitrary number of discrete grain-size classes. For a mixture of  $j$  constituents, the theory yields a system of  $j - 1$  independent segregation–remixing equations, which together with the summation condition can be used to determine the concentrations of each particle size. For a prescribed bulk velocity field, the resulting systems of parabolic equations can easily be solved using standard Galerkin finite

element methods that are available in programme libraries. This makes the theory extremely accessible to non-specialist users. An example Matlab m-file that uses the `pdepe` routine to solve for the steady-state segregation of a three-component mixture as it flows down a chute can be found in the online supplementary material.

Although the theory sets up a very useful framework in which to study size segregation, it does not give any further information about  $j(j-1)/2$  independent segregation rates, or the diffusive remixing coefficient, which are, in general, functions of the grain-size ratio, the absolute size of the particles, the shear rate, the normal pressure, the particle density and the local solids volume fraction. These dependencies must be determined by experiments or molecular dynamics simulations. A significant advantage of the current theory is that bi-disperse experiments and simulations can be used to determine the coefficients for the multi-component theory.

Multi-component segregation theory, where the diffusive remixing is neglected, is the natural generalization of the hyperbolic bi-disperse segregation theories of Gray & Thornton (2005) and Thornton *et al.* (2006). When there are three or more constituents, the system is not necessarily hyperbolic. For instance, a ternary mixture is guaranteed to be non-strictly hyperbolic only when the segregation rates lie in regions  $\Omega_1$ ,  $\Omega_2$  and  $\Omega_3$  of parameter space, defined by (5.10), (5.11) and (5.20). There is a fourth region  $\Omega_4$ , defined in (5.21), where the characteristic determinant can be positive or negative, indicating that the system may change from hyperbolic to elliptic, depending on the evolving concentrations. While such a change is not uncommon in steady-state problems, it leads to short-wavelength Hadamard instabilities and ill-posedness in time-dependent problems (Joseph & Saut 1990; Gray 1999; Goddard 2003).

Golick & Daniels (2009) experimentally observed that the segregation rate has a local maximum at a grain-size ratio of two, which suggests that region  $\Omega_4$  is a physically realistic region of parameter space. Fortunately, the diffusive effects of particle remixing are sufficient to regularize the theory. Numerical simulations show that the parabolic segregation-remixing equations are still linearly unstable for certain initial concentrations in region  $\Omega_4$ . These segregation-induced instabilities allow ‘sawtooth’ stripes to develop for short periods before being annihilated by growing regions of large and small particles at the surface and base of the flow. The instability may therefore be difficult to realize in physical experiments.

There are two fundamental types of segregation: inverse distribution grading, in which the entire grain-size population coarsens upwards (e.g. Cas & Wright 1987; Hiscott 2003), and reverse coarse-tail grading, where just the coarsest clasts inverse grade and a fine-grained matrix is found throughout the flow. Distribution grading occurs when the segregation rates  $S_{v\mu}$  are all comparable in magnitude. If the diffusive remixing is not too large, the avalanche sorts the grains into inversely graded layers, with high concentrations of large particles at the surface of the avalanche, high concentrations of fines at the bottom and the high concentrations of medium-sized particles sandwiched between the two. A physical example of this is shown in the rotating drum experiment in figures 1 and 2. The strength of the smooth transition between a layer of particles  $\nu$  that is adjacent to a layer of particles  $\mu$  is controlled by the Péclet number

$$Pe_{v\mu} = S_{v\mu}/D_r, \quad (11.1)$$

which determines the inverse length scale of the transition. For a mixture with a range of non-dimensional segregation rates  $S_{v\mu}$ , some of these transitions will be stronger than others, since the particles all experience the same amount of diffusive remixing

$D_r$ . In particular, if size class  $\nu$  is very close to size class  $\mu$ , then  $S_{\nu\mu}$  will be small, the Péclet number will be small, the length scale for the transition between the inversely graded layers will be large, and the segregation between these constituents will be very diffuse. This is why the segregation is weak in mixtures where there are many different size classes, which differ only by small increments in grain size. Mixtures with continuous size distributions can therefore suppress segregation (e.g. Newey *et al.* 2004; Jha & Puri 2010).

The non-diffuse theory yields simple insights into the process of size segregation in these systems. In this paper, an exact solution for the segregation of a ternary mixture from a homogeneously mixed inflow condition has been constructed, which is valid for all inflow concentrations provided that the segregation parameters lie in  $\Omega_3^+$ , which is defined in (8.60). The solution consists of six regions of constant concentration that are separated by eight shocks that accurately delineate the regions of high and low concentration at high Péclet numbers. It is also able to explain the nonlinear stretching effects that the prescribed velocity profiles have on the final heights of the inversely graded layers. This detailed understanding of the solution also leads to a very simple upper bound for the total segregation distance. This is equal to the segregation distance of the bi-disperse sub-mixture of medium and small grains, or large and medium grains, that segregates least well. The upper bound for the total segregation distance from a homogeneous inflow for cases that do not satisfy the existence conditions (8.51) has not been investigated. However, it is tempting to suppose that it is determined by the segregation distance of the pair of sub-mixtures, over the whole mixture, that segregate least well, i.e.

$$x_{total} \leq \max(x_{ls}, x_{lm}, x_{ms}) = \max\left(\frac{1}{S_{ls}}, \frac{1}{S_{lm}}, \frac{1}{S_{ms}}\right), \quad (11.2)$$

which is the natural extension of the result (8.72) to cases where  $x_{ls}$  can be greater than  $x_{lm}$  or  $x_{ms}$ . Indeed this concept is easily generalizable to a mixture with any number of constituents. This seems physically reasonable, but it is a conjecture, not a proved result.

The framework of multi-component size segregation theory also allows a simple exact solution for reverse coarse-tail grading to be constructed. Here the large- and medium-sized particles reverse grade, but the fine particle matrix is found everywhere. This shows that the introduction of a component that does not segregate well from any of the other constituents can significantly extend the distance for total segregation. Such mixtures exist, as geologists regularly see such grading in deposits from pyroclastic flows, but there is still considerable debate about the dominant segregation mechanisms in this case (Cagnoli & Manga 2005), as well as how the stationary deposits are related to the flowing avalanche (Branney & Kokelaar 1992). There may be considerable technological benefit in studying their properties, however, as they may suppress segregation sufficiently to keep granular materials reasonably well mixed when they flow over shorter distances.

This research was performed during two research visits to the Hydraulics Laboratory at EPFL Lausanne and was supported by generous funding from the School of Architecture, Civil and Environmental Engineering. Nico Gray also acknowledges support from NERC grants NER/A/S/2003/00439 and NE/E003206/1, as well as an EPSRC Advanced Research Fellowship GR/S50052/01 and GR/S50069/01. Christophe Ancey is grateful for the financial support provided by the Swiss National Science Foundation under grant number 200021-129538, the

competence centre in Mobile Information and Communication Systems (a centre supported by the Swiss National Science Foundation under grant number 5005-67322, MICS project), the competence centre in Environmental Sciences (TRAMM project) and the Swiss Federal Energy Agency.

Supplementary material is available at [journals.cambridge.org/flm](http://journals.cambridge.org/flm).

## REFERENCES

- ABRAMOWITZ, M. & STEGUN, I. 1970 *Handbook of Mathematical Functions*, 9th edn., §3.3.7. Dover.
- BAGNOLD, R. A. 1954 Experiments on gravity-free dispersion of large solid spheres in a Newtonian fluid under shear. *Proc. R. Soc. Lond. A* **225**, 49–63.
- BARTELT, P. & MCARDELL, B. W. 2009 Granulometric investigations of snow avalanches. *J. Glaciol.* **55** (193), 829–833.
- BAXTER, J., TÜZÜN, U., HEYES, D., HAYATI, I. & FREDLUND, P. 1998 Stratification in poured granular heaps. *Nature* **391**, 136.
- BERTRAN, P. 2003 The rock-avalanche of February 1995 at Claix (French Alps). *Geomorphology* **54**, 339–346.
- BRANNEY, M. J. & KOKELAAR, B. P. 1992 A reappraisal of ignimbrite emplacement: progressive aggradation and changes from particulate to non-particulate flow during emplacement of high-grade ignimbrite. *Bull. Volcanol.* **54**, 504–520.
- BRIDGWATER, J. 1976 Fundamental powder mixing mechanisms. *Powder Technol.* **15**, 215–236.
- CAGNOLI, B. & MANGA, M. 2005 Vertical segregation in granular mass flows: A shear cell study. *Geophys. Res. Lett.* **32**, L10402.
- CAGNOLI, B. & ROMANO, G. P. 2010 Effect of grain size on mobility of dry granular flows of angular rock fragments: An experimental determination. *J. Volcanol. Geotherm. Res.* **193** (1–2), 18–24.
- CALDER, E. S., SPARKS, R. S. J. & GARDEWEG, M. C. 2000 Erosion, transport and segregation of pumice and lithic clasts in pyroclastic flows inferred from ignimbrite at Lascar Volcano, Chile. *J. Volcanol. Geotherm. Res.* **104**, 201–235.
- CAS, R. A. & WRIGHT, J. V. 1987 *Volcanic Successions*. Allen & Unwin.
- CHADWICK, P. 1976 *Continuum Mechanics. Concise Theory and Problems*. Allen & Unwin.
- COLE, J. D. 1951 On a quasilinear parabolic equation occurring in aerodynamics. *Q. Appl. Maths* **9**, 225–236.
- COSTA, J. E. & WILLIAMS, G. 1984 Debris flow dynamics. *Tech. Rep.* 84–606. (Videotape) US Geological Survey.
- COURANT, R. & HILBERT, D. 1962 *Methods of Mathematical Physics*, vol. 2. Interscience.
- DADE, W. B. & HUPPERT, H. E. 1998 Long-runout rockfalls. *Geology* **26**, 803–806.
- DOLGUNIN, V. N. & UKOLOV, A. A. 1995 Segregation modelling of particle rapid gravity flow. *Powder Technol.* **83**, 95–103.
- DRAHUN, J. A. & BRIDGWATER, J. 1983 The mechanisms of free surface segregation. *Powder Technol.* **36**, 39–53.
- EHRICHS, E. E., JAEGER, H. M., KARCZMAR, G. S., KNIGHT, J. B., KUPERMAN, V. Y. & NAGEL, S. R. 1995 Granular convection observed by magnetic-resonance-imaging. *Science* **267**, 1632–1634.
- FÉLIX, G. & THOMAS, N. 2004 Relation between dry granular flow regimes and morphology of deposits: formation of levées in pyroclastic deposits. *Earth Planet. Sci. Lett.* **221**, 197–213.
- GODDARD, J. D. 2003 Material instability in complex fluids. *Annu. Rev. Fluid Mech.* **35**, 113–133.
- GOLICK, L. A. & DANIELS, K. E. 2009 Mixing and segregation rates in sheared granular materials. *Phys. Rev. E* **80** (4), 042301.
- GOIJON, C., DALLOZ-DUBRUJEAUD, B. & THOMAS, N. 2007 Bidisperse granular avalanches on inclined planes: A rich variety of behaviours. *Eur. Phys. J. E* **23**, 199–215.
- GRAY, J. M. N. T. 1999 Loss of hyperbolicity and ill-posedness of the viscous-plastic sea ice rheology in uniaxial divergent flow. *J. Phys. Oceanogr.* **29** (11), 2920–2929.
- GRAY, J. M. N. T. 2001 Granular flow in partially filled slowly rotating drums. *J. Fluid Mech.* **441**, 1–29.
- GRAY, J. M. N. T. 2010 Particle size segregation in granular avalanches: A brief review of recent progress. *AIP Conf. Proc.* **1227**, 343–362.

- GRAY, J. M. N. T. & ANCEY, C. 2009 Segregation, recirculation and deposition of coarse particles near two-dimensional avalanche fronts. *J. Fluid Mech.* **629**, 387–423.
- GRAY, J. M. N. T. & CHUGUNOV, V. A. 2006 Particle-size segregation and diffusive remixing in shallow granular avalanches. *J. Fluid Mech.* **569**, 365–398.
- GRAY, J. M. N. T. & HUTTER, K. 1997 Pattern formation in granular avalanches. *Contin. Mech. Thermodyn.* **9**, 341–345.
- GRAY, J. M. N. T. & KOKELAAR, B. P. 2010a Large particle segregation, transport and accumulation in granular free-surface flows. *J. Fluid Mech.* **652**, 105–137.
- GRAY, J. M. N. T. & KOKELAAR, B. P. 2010b Large particle segregation, transport and accumulation in granular free-surface flows – erratum. *J. Fluid Mech.* **657**, 539.
- GRAY, J. M. N. T., SHEARER, M. & THORNTON, A. R. 2006 Time-dependent solutions for particle-size segregation in shallow granular avalanches. *Proc. R. Soc. Lond. A* **462**, 947–972.
- GRAY, J. M. N. T., TAI, Y. C. & NOELLE, S. 2003 Shock waves, dead-zones and particle-free regions in rapid granular free-surface flows. *J. Fluid Mech.* **491**, 161–181.
- GRAY, J. M. N. T. & THORNTON, A. R. 2005 A theory for particle size segregation in shallow granular free-surface flows. *Proc. R. Soc. Lond. A* **461**, 1447–1473.
- GRAY, J. M. N. T., WIELAND, M. & HUTTER, K. 1999 Free surface flow of cohesionless granular avalanches over complex basal topography. *Proc. R. Soc. Lond. A* **455**, 1841–1874.
- GRIGORIAN, S. S., EGLIT, M. E. & IAKIMOV, YU. L. 1967 A new formulation and solution of the problem of snow avalanche movement. *Tr. Vysokogornogo Geofizicheskogo Instituta*, vol. 12, 104–113.
- GRUBER, U. & BARTELT, P. 2007 Snow avalanche hazard modelling of large areas using shallow water numerical methods and GIS. *Environ. Model. Softw.* **22** (10), 1472–1481.
- HERRMANN, H. J., MANTICA, G. & BESSIS, D. 1990 Space-filling bearings. *Phys. Rev. Lett.* **65** (26), 3223–3226.
- HILL, K. M., GIOIA, G. & AMARAVADI, D. 2004 Radial segregation patterns in rotating granular mixtures: Waviness selection. *Phys. Rev. Lett.* **93**, 224301.
- HILL, K. M. & KAKALIOS, J. 1995 Reversible axial segregation of rotating granular media. *Phys. Rev. E* **52** (4), 4393–4400.
- HILL, K. M., KHARKAR, D. V., GILCHRIST, J. F., MCCARTHY, J. J. & OTTINO, J. M. 1999 Segregation driven organization in chaotic granular flows. *Proc. Natl Acad. Sci. USA* **96**, 11701–11706.
- HISCOTT, R. N. 2003 In *Encyclopedia of Sediments and Sedimentary Rocks* (ed. G. V. Middleton), pp. 333–335. Springer.
- HOPF, E. 1950 The partial differential equation  $u_t + uu_x = \mu u_{xx}$ . *Commun. Pure Appl. Math.* **3**, 201–230.
- IVERSON, R. M. 1997 The physics of debris-flows. *Rev. Geophy.* **35**, 245–296.
- IVERSON, R. M. 2003 The debris-flow rheology myth. In *Debris-Flow Hazards Mitigation: Mechanics, Prediction and Assessment* (ed. D. Rickenmann & C. L. Chen), pp. 303–314. Millpress.
- IVERSON, R. M. & DENLINGER, R. P. 2001 Flow of variably fluidized granular masses across three-dimensional terrain. 1. Coulomb mixture theory. *J. Geophys. Res.* **106** (B1), 553–566.
- IVERSON, R. M., LOGAN, M., LAHUSEN, R. G. & BERTI, M. 2010 The perfect debris flow? aggregated results from 28 large-scale experiments. *J. Geophys. Res.* **115**, F03005.
- IVERSON, R. M. & VALLANCE, J. W. 2001 New views of granular mass flows. *Geology* **29** (2), 115–118.
- JHA, A. K. & PURI, V. M. 2010 Percolation segregation of multi-size and multi-component particulate materials. *Powder Technol.* **197** (3), 274–282.
- JOHANSON, J. R. 1978 Particle segregation ... and what to do about it. *Chem. Engng*, May, pp. 183–188.
- JOMELLI, V. & BERTRAN, P. 2001 Wet snow avalanche deposits in the French Alps: Structure and sedimentology. *Geografiska Annaler. A Phys. Geog.* **83**, 15–28.
- JOP, P., FORTERRE, Y. & POULIQUEN, O. 2006 A constitutive relation for dense granular flows. *Nature* **44**, 727–730.
- JOSEPH, D. D. & SAUT, J. C. 1990 Short-wave instabilities and ill-posed initial-value problems. *Theor. Comput. Fluid Dyn.* **1**, 191–227.
- KHAKHAR, D. V., MCCARTHY, J. J. & OTTINO, J. M. 1997 Radial segregation of granular mixtures in rotating cylinders. *Phys. Fluids* **9**, 3600–3614.

- KHAKHAR, D. V., MCCARTHY, J. J. & OTTINO, J. M. 1999 Mixing and segregation of granular materials in chute flows. *Chaos* **9**, 594–610.
- KYNCH, G. J. 1952 A theory of sedimentation. *Trans. Faraday Soc.* **48**, 166–176.
- LAX, P. D. 1957 Hyperbolic systems of conservation laws 2. *Commun. Pure Appl. Maths* **10** (4), 537–566.
- MAKSE, H. A., HAVLIN, S., KING, P. R. & STANLEY, H. E. 1997 Spontaneous stratification in granular mixtures. *Nature* **386**, 379–382.
- MANGENEY, A., BOUCHUT, F., THOMAS, N., VILOTTE, J. P. & BRISTEAU, M. O. 2007 Numerical modeling of self-channeling granular flows and of their levee-channel deposits. *J. Geophys. Res.* **112**, F02017.
- MAY, L. B. H., GOLICK, L. A., PHILLIPS, K. C., SHEARER, M. & DANIELS, K. E. 2010 Shear-driven size segregation of granular materials: Modeling and experiment. *Phys. Rev. E* **81** (5), 051301.
- MCCARTHY, J. J. 2009 Turning the corner in segregation. *Powder Technol.* **192** (2), 137–142.
- MIDDLETON, G. V. 1970 Experimental studies related to problems of flysch sedimentation. In *Flysch Sedimentology in North America* (ed. J. Lajoie), pp. 253–272. Business and Economics Science Ltd.
- MIDDLETON, G. V. & HAMPTON, M. A. 1976 Subaqueous sediment transport and deposition by sediment gravity flows. In *Marine Sediment Transport and Environmental Management* (ed. D. J. Stanley & D. J. P. Swift), pp. 197–218. Wiley.
- MORLAND, L. W. 1992 Flow of viscous fluids through a porous deformable matrix. *Surv. Geophys.* **13**, 209–268.
- NEWAY, M., OZIK, J., VAN DER MEER, S. M., OTT, E. & LOSERT, W. 2004 Band-in-band segregation of multidisperse granular mixtures. *Eur. Phys. Lett.* **66** (2), 205.
- PALLADINO, D. M. & VALENTINE, G. A. 1995 Coarse-tail vertical and lateral grading in pyroclastic flow deposits of the Latera Volcanic Complex (Vulsini, Central Italy): origin and implications for flow dynamics. *J. Volcanol. Geotherm. Res.* **69** (3–4), 343–364.
- PHILLIPS, J. C., HOGG, A. J., KERSWELL, R. R. & THOMAS, N. H. 2006 Enhanced mobility of granular mixtures of fine and coarse particles. *Earth Planet. Sci. Lett.* **246**, 466–480.
- PIERSON, T. C. 1986 Flow behavior of channelized debris flows, Mount St. Helens, Washington. In *Hillslope Processes* (ed. A. D. Abrahams), pp. 269–296. Allen & Unwin.
- PITMAN, E. B., NICHITA, C. C., PATRA, A., BAUER, A., SHERIDAN, M. & BURSİK, M. 2003 Computing granular avalanches and landslides. *Phys. Fluids* **15** (12), 3638–3646.
- POULIQUEN, O. 1999a Scaling laws in granular flows down rough inclined planes. *Phys. Fluids* **11** (3), 542–548.
- POULIQUEN, O. 1999b On the shape of granular fronts down rough inclined planes. *Phys. Fluids* **11** (7), 1956–1958.
- POULIQUEN, O., DELOUR, J. & SAVAGE, S. B. 1997 Fingering in granular flows. *Nature* **386**, 816–817.
- POULIQUEN, O. & VALLANCE, J. W. 1999 Segregation induced instabilities of granular fronts. *Chaos* **9** (3), 621–630.
- RHEE, H. K., ARIS, R. & AMUNDSON, N. R. 1986 *First-Order Partial Differential Equations, vol. 1: Theory and Applications of Single Equations*. Prentice-Hall.
- ROGNON, P. G., ROUX, J. N., NAAIM, M. & CHEVOIR, F. 2007 Dense flows of bidisperse assemblies of disks down an inclined plane. *Phys. Fluids* **19**, 058101.
- ROSATO, A., STRANDBURG, K. J., PRINZ, F. & SWENDSEN, R. H. 1987 Why the Brazil nuts are on top: Size segregation of particulate matter by shaking. *Phys. Rev. Lett.* **58** (10), 1038–1040.
- SAVAGE, S. B. & HUTTER, K. 1989 The motion of a finite mass of granular material down a rough incline. *J. Fluid Mech.* **199**, 177–215.
- SAVAGE, S. B. & LUN, C. K. K. 1988 Particle size segregation in inclined chute flow of dry cohesionless granular solids. *J. Fluid Mech.* **189**, 311–335.
- SCHRÖTER, M., ULRICH, S., KREFT, J., SWIFT, J. B. & SWINNEY, H. L. 2006 Mechanisms in the size segregation of a binary granular mixture. *Phys. Rev. E* **74** (1), 011307.
- SCHULZE, D. 2008 *Powders and Bulk Solids*. Springer.
- SCOTT, A. M. & BRIDGWATER, J. 1975 Interparticle percolation: A fundamental solids mixing mechanism. *Ind. Engng Chem. Fundam.* **14** (1), 22–27.
- SHEARER, M. & DAFERMOS, C. 2010 Finite time emergence of a shock wave for scalar conservation laws. *J. Hyperbolic Differ. Equ.* **7** (1), 107–116.

- SHEARER, M. & GIFFEN, N. 2010 Shock formation and breaking in granular avalanches. *Discr. Contin. Dyn. Sys.* **27** (2, Special Issue), 693–714.
- SHEARER, M., GRAY, J. M. N. T. & THORNTON, A. R. 2008 Stable solutions of a scalar conservation law for particle-size segregation in dense granular avalanches. *Eur. J. Appl. Maths* **19**, 61–86.
- SHINBROT, T. & MUZZIO, F. J. 1998 Reverse buoyancy in shaken granular beds. *Phys. Rev. Lett.* **81** (20), 4365–4368.
- SKEEL, R. D. & BERZINS, M. 1990 A method for the spatial discretization of parabolic equations in one space variable. *SIAM J. Sci. Stat. Comput.* **11** (1), 1–32.
- THORNTON, A. R. & GRAY, J. M. N. T. 2008 Breaking size-segregation waves and particle recirculation in granular avalanches. *J. Fluid Mech.* **596**, 261–284.
- THORNTON, A. R., GRAY, J. M. N. T. & HOGG, A. J. 2006 A three-phase mixture theory for particle size segregation in shallow granular free-surface flows. *J. Fluid Mech.* **550**, 1–25.
- TRUESDELL, C. 1984 *Rational Thermodynamics*. Springer.
- VALLANCE, J. W. & SAVAGE, S. B. 2000 Particle segregation in granular flows down chutes. In *IUTAM Symposium on Segregation in Granular Materials* (ed. A. D. Rosato & D. L. Blackmore), pp. 31–51. Kluwer.
- WHITHAM, G. B. 1974 *Linear and Nonlinear Waves*. John Wiley.
- WIEDERSEINER, S., ANDREINI, N., EPÉLY-CHAUVIN, G., MOSER, G., MONNEREAU, M., GRAY, J. M. N. T. & ANCEY, C. 2011 Experimental investigation into segregating granular flows down chutes. *Phys. Fluids* **23**, 013301.
- WILLIAMS, S. C. 1968 The mixing of dry powders. *Powder Technol.* **2**, 13–20.
- WILLS, B. A. 1979 *Mineral Processing Technology*. Pergamon.
- ZANUTTIGH, B. & DI PAOLO, A. 2006 Experimental analysis of the segregation of dry avalanches and implications for debris flows. *J. Hydraul. Res.* **44** (6), 796–806.
- ZANUTTIGH, B. & GHILARDI, P. 2010 Segregation process of water-granular mixtures released down a steep chute. *J. Hydrol.* **391** (1–2), 175–187.
- ZURIGUEL, I., GRAY, J. M. N. T., PEIXINHO, J. & MULLIN, T. 2006 Pattern selection by a granular wave in a rotating drum. *Phys. Rev. E* **73**, 061302.